A combined He-atom scattering and theoretical study of the low energy vibrations of physisorbed monolayers of Xe on Cu(111) and Cu(001)

A. Šiber and B. Gumhalter*

Institute of Physics of the University, P.O. Box 304, 10001 Zagreb, Croatia

J. Braun, A.P. Graham, M. F. Bertino and J.P. Toennies

Max-Planck-Institut für Strömungsforschung, Bunsenstrasse 10, D-37073 Göttingen, Germany

D. Fuhrmann and Ch. Wöll

Ruhr-Universität Bochum, Lehrstuhl für Physikalische Chemie I, Universitätstrasse 150, D-44801 Bochum, Germany

(February 6, 2008)

*Corresponding author. E-mail: branko@ifs.hr

Abstract

The surface phonon dispersion curves of commensurate Xe monolayers on Cu(111) and incommensurate Xe monolayers on Cu(001) surfaces have been measured using He atom scattering (HAS) time of flight (TOF) spectroscopy. The TOF spectra are interpreted by combining quantum scattering calculations with the dynamical matrix description of the surface vibrations. Both a vertically polarized Einstein-like mode and another, acoustic-like mode of dominantly longitudinal character, are identified. The latter mode is characterized by the presence and absence of the zone center frequency gap in the commensurate and incommensurate adlayers, respectively. The microscopic description of the TOF spectral intensities is based on the extensive theoretical studies of the interplay of the phonon dynamics, projectile-surface potentials, multi-quantum interference and projectile recoil, and their effect on the HAS spectra. Both single and multi-quantum spectral features observed over a wide range of He atom incident energies and substrate temperatures are successfully explained by the theory.

I. INTRODUCTION

In the past, investigations of physisorption potentials for particles on solid substrates as well as the potentials describing interadsorbate interactions were mainly motivated by the experimental studies of adsorption and phase transitions at surfaces. Several new developments have recently stimulated renewed interest. First, the possibility to manipulate and displace single atoms and molecules with low-temperature scanning tunneling microscopes [1,2] has not only added to our understanding of adsorbate-substrate interactions but also underlined the need for more detailed microscopic data. Second, the recent progress in understanding sliding friction [3] calls for more precise information on the potential energy surfaces and energy dissipation to the substrate [4]. Although physisorption energies can be determined in a rather straightforward fashion using thermal desorption spectroscopy (TDS), information on the interparticle potentials can be only extracted indirectly, either through precise analyses of the shape of TDS-peaks or by detailed investigations of phase transitions within the adsorbed adlayers [5].

As the interplay between adsorption and interadsorbate potentials determines the low energy dynamics of adlayers, studies of physisorbed rare gas monolayers are of special interest in the above discussed context because of their allegedly simple vibrational properties. In the present paper we describe a determination of the parameters of these potentials on the prototype commensurate and incommensurate physisorbed monolayers of Xe on Cu(111) and Cu(001), respectively, by using He atom scattering (HAS) time of flight (TOF) spectroscopy to measure the dispersion of the low-energy adlayer-modes in combination with a theoretical analysis of the scattering data. This provides direct information on the force constants which couple the adsorbates to the substrate, the effective corrugation of the potential energy surface (PES) describing the motion of the particles on the substrate, and the force constants coupling the adjacent adsorbates. Although the first HAS-TOF measurements on rare gas overlayers were carried out almost twenty years ago, these early experiments were only able to detect the vertically polarized Einstein-like S-mode [6,7]. Only recently was an

additional mode found for Xe on Cu(110) [8] and shortly thereafter also for Xe on Cu(001) [9], Cu(111) [10] and NaCl(001) [11] surfaces. This new mode was interpreted as being due to low-energy longitudinally polarized motion of the adsorbates. However, simple model calculations suggest a significant discrepancy between the fits based on this assignment [9,10] and empirical potential models used so far to model the adsorbate-adsorbate and adsorbate-substrate interactions. This has created some controversy in the literature [12] which calls for a critical reassessment of the HAS data on the low energy vibrations of physisorbed Xe monolayers.

In this paper we present the analysis of the experimental data obtained for a commensurate $(\sqrt{3} \times \sqrt{3})$R30° Xe adlayer adsorbed on Cu(111) and a similar system, viz. the hexagonal incommensurate Xe adlayer adsorbed on Cu(001). Measurements are reported on the dispersion curves and the excitation probabilities of two adlayer induced modes, the vertically polarized Einstein-like phonon branch over the entire surface Brillouin zone (SBZ) and the new in-the-surface plane polarized acoustic-like mode over the main part of the SBZ. In particular, for the latter mode in Xe/Cu(111) it was possible to measure the zone-center phonon gap which provides particularly important information on the Xe-substrate potential energy surface, and to compare this result to the recently published data on the incommensurate Xe-overlayer adsorbed on Cu(001) [9]. The first, tentative assignment of the modes observed in both systems was made by combining the symmetry selection rules applicable to the excitation of phonons of different polarization in the single phonon scattering regime with the results of lattice-dynamical analysis of the adlayers. This analysis showed that a good agreement between theoretical and experimental dispersion curves for Xe-induced modes could be obtained only with intralayer force constants derived from the Xe-Xe pair interaction unexpectedly softer than the one deduced from accurate gas phase potentials [13] or bulk phonon data [14]. As the use of this procedure was recently questioned [12], further progress in understanding the HAS data for monolayers of Xe on Cu(111) and Cu(001) necessitates resolving this controversy by carrying out a comprehensive and consistent analysis of the measured spectral features. Here we demonstrate that additional support to

the discussed assignments, and in particular of the dominantly longitudinal character of the observed acoustic mode, can be obtained by carefully examining the scattering intensities in the HAS TOF spectra. To this end we have performed detailed calculations of the absolute and relative excitation probabilities of the adlayer localized modes in the single and multiphonon scattering regime using a recently developed theoretical approach [15,16] and compared them with experimental HAS TOF intensities. A good agreement of the results of calculations with the experimental data provides a strong and convincing argument in favor of the present assignments and therefore of the strong modification of the monolayer force constants. It thereby points to some peculiar characteristics of the Xe-Xe interaction in adlayers of monoatomic thickness which still await a microscopic interpretation through detailed calculations of the adlayer electronic and structural properties.

The present article starts with a brief description of the experimental procedure and the preparation of Xe monolayers outlined in Sec. II. The experimental results are presented in Sec. III where a tentative assignment and interpretation of the modes observed in HAS from Xe monolayers on Cu(111) and Cu(001) is discussed. The theoretical model used to interpret the HAS TOF intensities measured both in the single and multiphonon scattering regimes is described in Sec. IV. The basic ingredients of the model relevant to the calculations of HAS from adlayers are discussed and illustrated for the example of realistic He-Xe interaction potentials. In Sec. V the experimental HAS TOF intensities are compared with the theoretical model predictions and physical implications of the good agreement are discussed. Section VI presents a way to determine the corrugation of the adlayer-substrate potential energy surface using the present approach. Finally, Sec. VII summarizes all the relevant findings and the most important conclusions. Preliminary reports on some results of the present work have been published previously [9,10].

II. EXPERIMENTAL

The experiments have been carried out in a high resolution helium atom scattering apparatus (base pressure 8×10^{-11} mbar, fixed total scattering angle θ_{SD}) described elsewhere [17]. The crystal was mounted on a home made crystal holder and the sample could be cooled down to 40 K with liquid helium. The sample temperatures were measured using a cromel-alumel thermocouple and could be stabilized to within ± 0.5 K. The Cu(111) crystal previously oriented to within 0.15° was cleaned by cycles of Ar ion sputtering (600 eV, 1μA/cm^2) followed by annealing at 1100 K. Prior to the experiments described here the cleanliness and the structural quality of the surface were checked by XPS and LEED. The 99.99% pure Xe gas was backfilled into the scattering chamber through a leak valve to a pressure of 4×10^{-8} mbar. During the preparation of the Xe monolayer structures the crystal temperature was kept at 70 K in order to avoid the formation of bi- and multilayers, which are stable only at temperatures below 68 K. For temperatures below 68 K the He-atom TOF spectra revealed the appearance of an additional loss, which could be assigned to vertically polarized vibrations of the second layer of Xe atoms. At the temperature of preparation of the Xe monolayer on Cu(111) the commensurate-incommensurate transitions are not expected as they have been detected to occur at around 47 K [18]. A description of the preparation of the Xe monolayer on the Cu(001) surface has been given in Refs. [9,19]

III. EXPERIMENTAL RESULTS

The right hand side of Fig. 1.a shows the structure of the commensurate $(\sqrt{3} \times \sqrt{3})$R30° monolayer of Xe atoms adsorbed on Cu(111) surface [20,21] and indicates the two principal directions (azimuths) of the substrate crystal surface. The left hand side (LHS) shows the first SBZ of the substrate (dashed lines) and the two dimensional Brillouin zone of the adlayer (full lines). Figure 1.b shows an angular distribution of He atoms scattered from $(\sqrt{3} \times \sqrt{3})$R30° Xe/Cu(111) surface for incident wave vector $k_i = 9.2$ Å^{-1} ($E_i = 45$ meV)

and the substrate temperature T_s=60 K along the $[1\bar{1}0]$-azimuth relative to the substrate surface. The intensities are normalized to the specular peak height. In addition to the (1,0) diffraction peak, two additional, Xe (1/3,0) and (2/3,0) diffraction peaks of the order one-third were observed [19]. The sharpness of the peaks and relatively low background indicate the presence of a well-ordered, largely defect-free Xe-overlayer.

Figure 2 shows an angular distribution along the substrate [100]-azimuth obtained by scattering He atoms from a monolayer of Xe atoms adsorbed on Cu(001) for incident wave vector $k_i = 5.25$ Å^{-1} ($E_i = 14.36$ meV) and T_s=52 K. This distribution indicates a well defined structure. The earlier LEED studies at $T_s \geq 77$ K have identified a hexagonally ordered adlayer incommensurate with the underlying substrate [22,23], so as that the [100] substrate direction lies along equivalent non-high symmetry directions for the two domains of the Xe monolayer, one rotated by 30^0 from the other. The geometrical structure of these domains is shown in Fig. 6 of Ref. [22] and Fig. 2 of Ref. [23]. The present out-of-the-high-symmetry-plane measurements indicate sharp diffraction peaks commensurate with the orientation of the Xe overlayer along the Cu(001) [110] azimuth except for the two bumps at each side of the specular peak. Their presence is related to inelastic resonance processes involving the Cu(001) surface Rayleigh wave and intense nondispersive Xe mode with polarization perpendicular to the surface, as determined by the TOF measurements described below. These characteristics of He-angular distribution spectra from Xe/Cu(001) for $T_s < 65$ K indicate a "floating" incommensurate Xe adlayer. Hence, in the case of both Cu substrates the Xe adlayers may be considered planar and periodic with hexagonal symmetry, irrespective of the (in)commensurability with the underlying substrate. The periodicity and symmetry of the adlayers is then reflected in their vibrational properties. The adlayer vibrational modes can be classified as dominantly in-plane polarized (longitudinal (L) and shear horizontal (SH)) and shear vertical (S) [24].

Figure 3 shows typical He atom TOF spectra for the $(\sqrt{3} \times \sqrt{3})$R30°Xe/Cu(111) surface along the $[11\bar{2}]$ substrate azimuth (i.e. along the $\bar{\Gamma}\bar{\mathrm{K}}_{Xe}$ direction of the superstructure), for $\theta_{SD} = \theta_i + \theta_f = 90.5^0$ and three different He atom incident energies E_i spanning the

transition from the single to the multi-quantum scattering regime. The TOF spectra have been converted from flight time to energy transfer scale. Arbitrary units are used for spectral intensities on the vertical axis. The spectrum at the lowest incident energy (E_i=9.9 meV) is typical of the single phonon scattering regime and is dominated by two well defined peaks at $\pm$2.62 meV on the energy loss and gain sides of the TOF spectrum, respectively. Within the experimental error these energies do not change in the interval beyond $\Delta K = 0.1$ Å^{-1} in the first SBZ of the superstructure. In accordance with previous works on noble gas atoms adsorbed on other substrates [7,26], this mode is assigned to the excitation of collective vibrations of Xe-atoms with a polarization vector vertical to the surface and is designated the S-mode. The lack of dispersion indicates that the frequency of the vertically polarized phonon is mainly determined by the adsorbate coupling to the substrate, with only a weak coupling to adjacent adsorbates. Deviation from a dispersionless behavior occurs only at the intersection with the substrate Rayleigh-mode [25,26]. The energy of this S-mode ($\hbar\omega_S = 2.62$ meV), is slightly larger than for the (110)-face of Cu ($\hbar\omega_S = 2.5$ meV [8]). The small, but significant deviation of 0.12 meV is consistent with a slightly deeper potential well for Xe on Cu(111) and Cu(001) than on Cu(110) [27,28].

In addition to the intense S-peaks the measured spectrum also reveals the presence of a weak but clearly resolved feature (labeled "L") near the elastic or zero energy loss line. The energy of this mode changes with the angle of incidence θ_i and thus shows dispersion. The spectral intensity of this mode relative to that of the S-mode in each TOF measurement was found to decrease strongly with the magnitude of its wave vector so that for the He$\rightarrow$Xe/Cu(111) system the corresponding data points could only be obtained for parallel wavevector up to one third of the distance between the $\bar{\Gamma}$ and $\bar{\mathrm{K}}_{Xe}$ points in the first Brillouin zone of the superstructure (interval shown in Fig. 5). Since in the displayed TOF spectra the energy of the "L" mode is always significantly below that of the lowest surface phonon of the clean Cu(111) surface [29], this must be a pure Xe adlayer-induced mode which cannot couple to the substrate for wavevectors over a wide range of the SBZ. As for the $(\sqrt{3}\times\sqrt{3})$R30° Xe/Cu(111) system the [11$\bar{2}$] direction has a high symmetry mirror

plane the vibrational modes are partitioned in two orthogonal classes [30]. Two thirds of the modes are polarized in the sagittal plane (including the adlayer induced S- and L-modes). The remaining one third of the modes are polarized in the surface plane and normal to the mirror plane and designated shear horizontal or SH-modes. The three possible adlayer induced orthogonal modes with the wavevector in the $[11\bar{2}]$ direction (c.f. Fig. 1.a) are thus characterized by either a combination of the components with S- and L-polarization or pure SH-polarization. Combining the symmetry selection rules pertinent to the probabilities of excitation of in-plane phonons at ideal surfaces (c.f. Refs. [31,32] and Sec. IV below) with the fact that the data were recorded in the first SBZ of the superstructure and in the sagittal plane which coincides with the high symmetry plane of the Xe/Cu(111) system, the observation of the SH-mode under these experimental conditions can be ruled out. Hence, this mode is tentatively assigned to the longitudinal mode of the adlayer which is known to couple to the scattered He atoms under similar conditions [31,32]. However, as demonstrated for NaCl, the SH-modes *can* be excited along a high symmetry direction in the *second* SBZ [33].

The other two spectra in Fig. 3 demonstrate the transition from a single to a multiphonon scattering regime as E_i is increased. This transition takes place already at rather low He atom incident energies due to the very low excitation energies of the adlayer-induced S-modes whose vertical polarization gives rise to a strong projectile-phonon coupling (c.f. Sec. IV). Although some single phonon features are still discernible at incident energy $E_i = 21.4$ meV, both spectra are dominated by a number of uniformly spaced peaks at energies $\pm n \times 2.62$ meV. For $E_i = 45.1$ meV the true multiphonon scattering regime is reached because the intensity of the elastic peak is smaller than that of the multi-quantum S-peak for $n = 2$.

Figure 4 shows three representative He-atom time-of-flight spectra for the incommensurate Xe monolayer on Cu(001) for three different He atom incident energies along the $\langle 100 \rangle$ substrate azimuth which lies halfway between the two high symmetry directions of the adlayer SBZ. In all essential aspects these spectra are similar to those shown in Fig. 2. They also exhibit strong dispersion of the "L" mode and the multiple excitation of S-modes

at energies $\pm n \times 2.71$ meV. In addition, the Rayleigh mode (labeled RW) of the underlying Cu(001) substrate is also observed at low and intermediate energies E_i. The RW dispersion curves of clean Cu(111) and Cu(001) surfaces are well known from the previous work [25,29].

It is noteworthy that for both adlayers the multiphonon lines are all, to within experimental error, located at integral multiples of a fundamental frequency ω_S, 2.62 meV/$\hbar$ for Xe/Cu(111) and 2.71 meV/$\hbar$ for Xe/Cu(001). At the first sight this seems to imply a very harmonic Xe-Cu potential since anharmonic shifts, which are expected to be negative, would produce overtone energies smaller than the corresponding multiples of the fundamental frequency ω_S (c.f. Sec. VI). However, the theoretical analyses of the Xe-metal interactions [27,28,34] show that the potential is notably anharmonic but, as we show in the next sections, the multiple spectral peaks can be explained by multiple excitation of delocalized phonon modes which involve the lowest harmonic states of many adatoms rather than a single higher anharmonic state localized on a single adatom. In this case there is no anharmonic shift as each multiphonon excitation is distributed over several Xe atoms in the overlayer.

From up to about a couple of hundred of TOF spectra with different θ_i the experimental dispersion curves were determined and are shown in Figs. 5 and 6. For both Xe/Cu(111) and Xe/Cu(001) the vertically polarized S-mode exhibits negligible dispersion over the major part of the SBZ except at the point of avoided crossing with the substrate RW [35]. The most striking difference between the vibrational dynamics of the two adsorbate phases manifests itself in the dispersion of the "L" mode. The "L" mode for the commensurate Xe/Cu(111) structure exhibits a zone center gap of about 0.4 ± 0.1 meV whereas for the incommensurate phase the frequency at the zone center goes to zero linearly with the wave vector.

To further aid the assignments of the modes in the He→Xe/Cu(111) TOF spectra and analyze their dispersion we have carried out a full lattice dynamics calculation of the vibrationally coupled $(\sqrt{3} \times \sqrt{3})$R30° Xe/Cu(111) system with Xe atoms placed in on-top sites on both sides of a 40 layer thick slab of substrate atoms and interadsorbate distance $d^{Xe-Xe} = 4.42$ Å. The interaction between nearest-neighbor Cu atoms was accounted for by a single radial force constant $\beta^{Cu} = 28.0$ N/m as obtained from a fit of the bulk Cu phonon

dispersion curves [36]. The other parameters describing the coupling of the Xe atoms to the nearest neighbor Cu substrate atoms was fitted to the dispersion curves, which yielded a radial force constant $\beta^{Xe} = 3.7$ N/m and a tangential force constant $\alpha^{Xe} = 0.086$ N/m. Assigning the longitudinal character to the observed "L" mode to comply with the above discussed symmetry selection rules, the interaction between the atoms in the adlayer could be described by a radial force constant $\beta^{Xe-Xe} = 0.5$ N/m and a tangential force constant $\alpha^{Xe-Xe} = 0$. The results of the full calculation are shown in Fig. 9 in the next section and in Fig. 5 we present only the dispersion for the surface projected S- and longitudinal modes which reproduce the experimental data very satisfactorily. The radial Xe-Xe force constant $\beta^{Xe-Xe} = 0.5$ N/m resulting from this procedure is, however, significantly smaller than the value predicted from the highly precise HFD-B2 gas-phase potential [13], $\beta^{Xe-Xe}_{HFD} = 1.67$ N/m, which produces a significantly steeper dispersion curve for longitudinal phonons denoted by dash-dotted curve in Fig. 5.

In the case of incommensurate monolayer of Xe on Cu(001) it was only possible to set up a three-dimensional dynamical matrix describing the three vibrational modes localized in the adlayer, namely the S-, L- and SH-modes (c.f. Refs. [7,24]). Since the experimental data were taken halfway between the two high symmetry directions of the two dimensional hexagonal Xe adlayer Brillouin zone, the broken symmetry no longer forbids excitation of the SH-mode. However, since the calculated polarization vector of the SH-mode is nearly perpendicular and of the L-mode nearly parallel to the present azimuthal direction [37], the corresponding excitation probabilities of the SH-phonon are expected to be much smaller than those of the L-phonon (c.f. Refs. [31,32] and Sec. IV). Hence, as in the case of the commensurate system, a longitudinal polarization is assigned to the observed low energy adlayer-induced acoustic "L" mode also in the incommensurate system Xe/Cu(001). The interadsorbate distance was fixed at $d^{Xe-Xe} = 4.40$ Åand the best-fit force constants in the [001] direction are: $\beta^{Xe} = 3.8$ N/m, $\beta^{Xe-Xe} = 0.42$ N/m, and $\alpha^{Xe-Xe}_T = 0.012$ N/m, which are similar to force constants for the Cu(111) substrate. These results are also presented in Fig. 6 and reproduce the experimental data very well. For comparison the dispersion of the

L-mode calculated by using β_{HFD}^{Xe-Xe} is also shown as a dash-dotted line and does not fit to the data. However, in the case of both Xe adlayers, the physical origin of the unexpected large softening of the radial Xe-Xe force constants introduced to reconcile the symmetry requirements with the experimental data remains unclear. A clue to this effect in the case of Cu(001) and Cu(111) surfaces may be provided by their peculiar electronic structure which gives rise to surface electronic states with corresponding electronic wave functions extending far across the adsorbed Xe atoms [38]. Alternatively, a delocalization of the electronic charge within the monolayer itself could give rise to softening of intralayer forces which then might explain the same phenomenon observed for an insulating substrate like NaCl(001) [11].

Recently, it was suggested that the observed "L"-mode could be interpreted as a SH-mode as this would be consistent with a thermodynamic analysis of the Xe/Cu(001) system [12]. This has created the controversy in the literature referred to in the Introduction and additionally motivated the present study. However, the model calculations of the HAS-TOF intensities reported in the next sections do not support such an interpretation.

IV. THEORETICAL DESCRIPTION OF He ATOM SCATTERING FROM Xe ADLAYERS ON Cu(001) AND Cu(111)

Since the assignments of the peaks in the experimental TOF spectra discussed in the preceding section have been questioned [12] additional corroboration by theoretical arguments is called for. To this end we have carried out extensive calculations based on the recently developed fully quantum model of inelastic He atom-surface scattering [15,16,39,40] which is especially suitable for scattering from adlayers [10,19,41]. In this model, the single and multiphonon excitation processes can be treated on an equivalent footing without invoking additional quasi-classical approximations for the scattered particle dynamics [42,43]. A detailed description of the model was presented in Ref. [15], so only its salient properties relevant to the calculations of HAS from adlayers are outlined here.

In view of the HAS angular distributions characteristic of the present Xe/Cu(111) and

Xe/Cu(001) surfaces (c.f. Figs. 1 and 2), the static corrugation of the He-surface interaction potential will be neglected so that the Xe overlayers are assumed to be flat and free of defects. The assumption of a planar and perfectly periodic Xe adlayer justifies the use of the dynamical matrix approach in the description of the vibrational properties of the surface in terms of phonon modes characterized by their parallel wave vector and branch index. The model Hamiltonian describing inelastic atom-surface collisions can then be cast in the form:

$$H = H_0^{part} + H_0^{ph} + V(\mathbf{r}), \tag{1}$$

where

$$H_0^{part} = \frac{\mathbf{p}^2}{2M} + U(z) \tag{2}$$

is the Hamiltonian describing unperturbed motion of the projectile in the flat static potential $U(z)$ of the target. The projectile particle is characterized by its coordinate and momentum operators $\mathbf{r} = (\boldsymbol{\rho}, z)$ and $\mathbf{p} = (\mathbf{P}, p_z)$, respectively, and mass M. Here $\boldsymbol{\rho}$, z and $\mathbf{P}$, p_z denote the parallel (lateral) and vertical (normal) to the surface components of $\mathbf{r}$ and $\mathbf{p}$, respectively. H_0^{ph} is the Hamiltonian of the unperturbed phonon field which can be constructed once the dispersion and polarization of the vibrational modes of the Xe/Cu system are known, and $V(\mathbf{r})$ is the dynamic projectile-surface interaction. The distorted waves $\langle \mathbf{r} \mid \mathbf{k} \rangle = \langle \boldsymbol{\rho}, z \mid \mathbf{K}, k_z \rangle$, which are the eigenstates of H_0^{part}, are described by the quantum numbers $\mathbf{K} = \mathbf{P}/\hbar$ and $k_z = p_z/\hbar$ denoting, respectively, the asymptotic parallel and normal projectile wave vectors far outside the range of the potential $U(z)$. The corresponding unperturbed energy of the projectile is then given by $E_{\mathbf{k}} = \hbar^2(\mathbf{K}^2 + k_z^2)/2M$. Using the box normalization these eigenstates can be orthonormalized to satisfy $\langle \mathbf{k} \mid \mathbf{k}' \rangle = \delta_{\mathbf{k},\mathbf{k}'}$, and are except for a phase factor equal to the unperturbed incoming and outgoing states satisfying the scattering boundary conditions [31]. Explicitly, for a flat surface we have, in the coordinate representation,

$$\langle \mathbf{r} \mid \mathbf{k} \rangle = \frac{e^{i\mathbf{K}\boldsymbol{\rho}} \chi_{k_z}(z)}{\sqrt{L_z L_s^2}}, \tag{3}$$

where L_s and L_z are the quantization lengths in the parallel and perpendicular to the surface directions, respectively, and $\chi_{k_z}(z)$ satisfies the limit $\chi_{k_z}(z \to \infty) \to 2\cos(k_z z + \eta)$. A more detailed description of the distorted wave scattering formalism was given in Refs. [31,32,44–46].

The theoretical description of the scattering event described by Hamiltonian (1) is sought in terms of a scattering spectrum $N(\Delta E, \Delta\mathbf{K})$, which gives the probability density that an amount of energy ΔE and parallel momentum $\hbar\Delta\mathbf{K}$ are transferred from the He atom to the substrate phonon field. The particular choice of these two variables is dictated by the symmetry of the problem, the conservation of the total energy and, for a periodic surface, the conservation of the parallel momentum to within a reciprocal lattice vector $\mathbf{G}$. Therefore, ΔE and $\Delta\mathbf{K}$ completely determine the final state of the scattered particle provided its initial state $\mathbf{k_i} = (\mathbf{K_i}, k_{zi})$ is well specified. With these prerequisites the energy and parallel momentum resolved scattering spectrum is defined by [15,39,40,44,47–49]

$$N_{\mathbf{k_i}}(\Delta E, \Delta\mathbf{K}) = \lim_{t\to\infty} \langle \Psi(t) \mid \delta[\Delta E - (H_0^{ph} - \varepsilon_i)]\delta(\hbar\Delta\mathbf{K} - \hat{\mathbf{P}}^{ph}) \mid \Psi(t)\rangle, \tag{4}$$

where $\hat{\mathbf{P}}^{ph}$ is the parallel momentum operator of the unperturbed phonon field, ε_i is the initial energy of the phonon field, $\Delta\mathbf{K} = \mathbf{K_i} - \mathbf{K_f}$, and $\mid \Psi(t)\rangle$ is the wave function of the entire interacting system. For calculational convenience, the phonon creation (annihilation) processes are assigned positive (negative) ΔE and $\Delta\mathbf{K}$ since they refer to the phonon field quantum numbers. The corresponding experimental quantities have, however, opposite signs because they refer to the measured changes of energy and parallel momentum of the projectile. The spectrum (4) is inherently normalized to unity and hence satisfies the optical theorem. It is also directly proportional to the experimental time-of-flight (TOF) spectrum [16]. Based on the translational symmetry of the system we shall in the following describe the phonon modes propagating in Xe monolayers by their wave vector $\mathbf{Q}$ parallel to the surface, branch index j, polarization vector $\mathbf{e}(\mathbf{Q}, j)$ and energy $\hbar\omega_{\mathbf{Q},j}$ [7,24]. The problem of localized modes characteristic of either mixed layers with broken or reduced translational symmetry [50] or of isolated adsorbates will be treated elsewhere.

Under the conditions in which the HAS experiments were carried out, the uncorrelated phonon exchange processes dominate over the correlated ones [15]. Then the angular resolved scattering spectrum is accurately represented by the expression:

$$N^{EBA}_{\mathbf{k_i},T_s}(\Delta E,\Delta\mathbf{K}) = \int_{-\infty}^{\infty} \frac{d\tau d^2\mathbf{R}}{(2\pi\hbar)^3} e^{\frac{i}{\hbar}[(\Delta E)\tau - \hbar(\Delta\mathbf{K})\mathbf{R}]} \exp[2W^{EBA}(\mathbf{R},\tau) - 2W^{EBA}(0,0)], \quad (5)$$

where τ and $\mathbf{R} = (X, Y)$ are auxiliary variables occurring after the temporal and spatial Fourier representation of the energy and parallel momentum delta-functions, respectively, are introduced on the RHS of expression (4) [15], $2W^{EBA}(\mathbf{R},\tau)$ is the exponentiated Born approximation (EBA) expression for the so-called scattering or driving function which contains all information on uncorrelated phonon exchange processes in the atom-surface scattering event. Its zero point value $2W^{EBA}(0,0) = 2W^{EBA}_{T_s}$ gives the Debye-Waller exponent (DWE) in the EBA and the corresponding Debye-Waller factor (DWF), $\exp[-2W^{EBA}_{T_s}]$, gives the probability of the elastically scattered specular beam [51]. Since in the EBA the correlations between two subsequent phonon scattering events are neglected, the expression for $N^{EBA}_{\mathbf{k_i},T_s}(\Delta E,\Delta\mathbf{K})$ on the LHS of (5) must be combined with the conservation laws for the total energy and parallel momentum [52].

The EBA expression for the scattering spectrum (5) holds irrespective of the form of the projectile-phonon coupling. However, it has been shown [53] that, for the projectile-phonon coupling to all orders in the lattice displacements, the higher order phonon exchange processes which involve only single phonon vertices and originate from linear coupling give much larger contribution to the scattering matrix than the non-linear many-phonon processes of the same multiplicity (c.f. Fig. 1 of Ref. [53] and Fig. 1 of Ref. [15]). Hence, in the present approach, only the linear projectile-phonon coupling will be retained, in which case the scattering function takes the form [15]:

$$2W^{EBA}(\mathbf{R},\tau) = \sum_{\mathbf{Q},\mathbf{G},j,k'_z} \Big[\mid \mathcal{V}^{\mathbf{K_i},\mathbf{Q}+\mathbf{G},j}_{k'_z,k_{zi}}(+) \mid^2 [\bar{n}(\hbar\omega_{\mathbf{Q},j}) + 1] e^{-i(\omega_{\mathbf{Q},j}\tau - (\mathbf{Q}+\mathbf{G})\mathbf{R})} + \\ + \mid \mathcal{V}^{\mathbf{K_i},\mathbf{Q}+\mathbf{G},j}_{k'_z,k_{zi}}(-) \mid^2 \bar{n}(\hbar\omega_{\mathbf{Q},j}) e^{i(\omega_{\mathbf{Q},j}\tau - (\mathbf{Q}+\mathbf{G})\mathbf{R})} \Big]. \quad (6)$$

Here $\bar{n}(\omega_{\mathbf{Q},j})$ is the Bose-Einstein distribution of phonons of energy $\hbar\omega_{\mathbf{Q},j}$ at the substrate

temperature T_s and the symbols

$$\mathcal{V}^{\mathbf{K_i},\mathbf{Q}+\mathbf{G},j}_{k'_z,k_{zi}}(\pm) = 2\pi V^{\mathbf{K_i}\mp\mathbf{Q}+\mathbf{G},\mathbf{K_i},j}_{k'_z,k_{zi}}\delta(E_{\mathbf{K_i}\mp\mathbf{Q}+\mathbf{G},k'_z} - E_{\mathbf{K_i},k_{zi}} \pm \hbar\omega_{\mathbf{Q},j}) \tag{7}$$

denote the on-the-energy and momentum-shell one-phonon emission (+) and absorption (−) matrix elements or the probability amplitudes of inelastic He atom-surface scattering [15] expressed through the corresponding off-the-energy-shell interaction matrix elements $V^{\mathbf{K_i}\mp\mathbf{Q}+\mathbf{G},\mathbf{K_i},j}_{k'_z,k_{zi}}$ (see below). In the present fully three dimensional calculations the wave vectors of real phonons exchanged in the collision will be restricted to the first SBZ of the superstructure (i.e. $\mathbf{G}$=0) because the major part of the experimental data was recorded in this region. However, for integrated quantities such as the DWF, the relevant summations sometimes need to be extended beyond the first SBZ (see below). The matrix elements given by expression (7) are normalized to unit particle current normal to the surface, $j_z = v_z/L_z = \hbar k_z/ML_z$. This can be easily verified if according to the box normalization the energy conserving δ-function in (7) is converted into the Kronecker symbol following the identity

$$2\pi\delta(E_{\mathbf{K}\mp\mathbf{Q},k'_z} - E_{\mathbf{K},k_z} \pm \hbar\omega_{\mathbf{Q},j}) = \frac{L_z}{\hbar\sqrt{v'_z v_z}}\delta_{k'_z,\bar{k}_{zi}}\Theta(\bar{k}^2_{zi}), \tag{8}$$

where $\bar{k}^2_{zi} = \pm 2\mathbf{K_i}\cdot\mathbf{Q} - \mathbf{Q}^2 + k^2_{zi} \mp 2M\omega_{\mathbf{Q},j}/\hbar$ and $\Theta(\bar{k}^2_{zi})$ is the step function restricting $\bar{k}^2_{zi}$ only to open scattering channels in which $\hbar k'^2_z/2M > 0$. The factor of L_z appearing in (8) is canceled by the factor L_z^{-1} appearing in $V^{\mathbf{K_i}\mp\mathbf{Q},\mathbf{K_i},j}_{k'_z,k_{zi}}$ which arises from the box normalization of the projectile wave functions (c.f. Eq. (3)). This enables a straightforward summation over k'_z on the RHS of expression (6). The quantization lengths in the parallel directions also cancel out from expression (6) after the final summation over $\mathbf{Q}$. The Debye-Waller exponent is then obtained from Eq. (6) by a straightforward substitution $\mathbf{R} = 0$ and $\tau = 0$.

In the following we shall adopt for $V^{\mathbf{K_i}\mp\mathbf{Q},\mathbf{K_i},j}_{k'_z,k_{zi}}$ the expressions obtained by taking the matrix elements of the vibrating part $V(\mathbf{r})$ of the total He-Xe/Cu potential $V_{tot}(\mathbf{r})$ which will be modeled by a pairwise sum [54] of atomic He-Xe interaction potentials $v(\mathbf{r} - \mathbf{r_l})$ [55,56]. Hence:

$$V(\mathbf{r}) = (V_{tot}(\mathbf{r}))_{vib} = \left(\sum_{\mathbf{l}} v(\mathbf{r} - \mathbf{r_l} - \mathbf{u_l}) \right)_{vib}, \tag{9}$$

where $\mathbf{r_l} = (\boldsymbol{\rho_l}, z_l)$ ranges over the equilibrium positions of Xe atoms and $\mathbf{u_l}$ denotes the displacement of the $\mathbf{l}$-th Xe atom from equilibrium. The static part of $V_{tot}(\mathbf{r})$, which is equal to the average of the pairwise sum in the brackets on the RHS of Eq. (9), is then identified with the static atom-surface potential $U(z)$ which is included in H_0^{part} in Eq. (2). The thus formulated scattering theory is equally appropriate to treat single and multiphonon scattering processes in HAS and incorporates the single phonon DWBA scattering theory reviewed in Refs. [31] and [32] as a special limit.

To simplify the numerical calculations and in particular the treatment of the interaction matrix elements and the scattering function, we shall approximate $U(z)$ by a suitably adjusted Morse potential:

$$U(z) = D(e^{-2\alpha(z-z_0)} - 2e^{-\alpha(z-z_0)}), \tag{10}$$

where D, z_0 and α denote the potential well depth, position of the minimum and the inverse range, respectively. This approximation is justified in the range of energies of the present HAS experiments [57]. The values of these potential parameters appropriate to the two studied collision systems are given in Sec. V in which they are explicitly quoted as the input in the calculations of the scattering intensities for comparison with the experimental results.

Following the findings of Ref. [58] that the repulsive and attractive components of the pair potentials contribute to the vibrating part of the total dynamic atom-surface interaction, both components are included in the dynamic atom-adlayer interaction. Then the matrix elements for linear atom-phonon coupling acquire a simple form [31,32]:

$$V_{k_z', k_z}^{\mathbf{K} \mp \mathbf{Q}, \mathbf{K}, j} = \mathbf{u}^*(\mathbf{Q}, j) \cdot \mathbf{F}(\mathbf{K}' - \mathbf{K}, k_z', k_z) \delta_{\mathbf{K}', \mathbf{K} \mp \mathbf{Q}}, \tag{11}$$

where $\mathbf{u}(\mathbf{Q}, j)$ is the vector of quantized displacement of the adlayer atoms corresponding to the phonon mode $(\mathbf{Q}, j)$ defined below in Eq. (15). The parallel momentum conserving Kronecker symbols $\delta_{\mathbf{K}', \mathbf{K} \mp \mathbf{Q}}$ arise as a result of the summation over adsorption sites of pair

potential contributions from all adsorbates in the periodic adlayer. The matrix element of the force $\mathbf{F}(\mathbf{K}'-\mathbf{K},k_z',k_z)$ exerted on the projectile by an atom in the adlayer is expressed as [31,32]:

$$\mathbf{F}(\mathbf{K}'-\mathbf{K},k_z',k_z)=\langle\chi_{k_z'}\mid(i(\mathbf{K}'-\mathbf{K}),-\partial/\partial z)v(\mathbf{K}'-\mathbf{K},z)\mid\chi_{k_z}\rangle, \tag{12}$$

where $v(\mathbf{K}'-\mathbf{K},z)$ is a two-dimensional Fourier transform of $v(\mathbf{r})$ which appears in expression (12) after taking the matrix element between the parallel components of the projectile wave functions $\langle\boldsymbol{\rho}\mid\mathbf{K}'\rangle$ and $\langle\boldsymbol{\rho}\mid\mathbf{K}\rangle$. The scalar product appearing in expression (11) gives the afore mentioned symmetry selection rules for excitation amplitudes of the various one-phonon scattering processes. In particular, for a purely SH-polarized phonon with a polarization vector in the surface plane and perpendicular to the mode wave vector $\mathbf{Q}$ in the first SBZ, the scalar product in (11) will be equal to zero, leading to a vanishing excitation probability. Expressions (11) and (12) also indicate that for small parallel momentum transfer to phonons the projectile-phonon coupling is strongest for vibrations with polarization vector perpendicular to the surface.

The parallel or $(\mathbf{K}'-\mathbf{K})$-dependence of $v(\mathbf{K}'-\mathbf{K},z)$ was modeled by introducing the cut-off wave vector Q_c which gives an approximate upper bound on the parallel momentum transfer in the one-phonon exchange processes (Hoinkes-Armand effect [59]). Denoting $\mathbf{K}'-\mathbf{K}=\mathbf{Q}$ this yields:

$$v(\mathbf{Q},z)=D(e^{-2\alpha(z-z_0)}e^{-Q^2/2Q_c^2}-2e^{-\alpha(z-z_0)}e^{-Q^2/Q_c^2}). \tag{13}$$

with the property $v(\mathbf{Q}=0,z)=U(z)$. The appearance of different effective cut-offs in the Q-dependence of the repulsive and attractive components of $v(\mathbf{Q},z)$ in Eq. (13) (viz. $\sqrt{2}Q_c$ versus Q_c) is a consequence of the different ranges of the repulsive and attractive components of the model pair potential $v(\mathbf{r}-\mathbf{r_l})$ consistent with expression (10) [58]. In the case of exponential potentials of range $1/\beta$ the value of Q_c is approximately given by [54]:

$$Q_c=\sqrt{\frac{\beta}{z_t}}, \tag{14}$$

where z_t is the (energy dependent) average value of the He atom turning point in the surface potential $U(z)$. Although the numerical evaluation of the matrix elements (12) avoids the explicit introduction of Q_c [57] the effect of the cut off in the parallel momentum transfer remains [60]. The matrix elements described by Eq. (12) were all calculated by using the pair potentials $v(\mathbf{r}-\mathbf{r_l})$ to obtain $v(\mathbf{Q},z)$, Eq. (13), with the parameters corresponding to the two studied systems explicitly defined in the next section. Figures 7.a and 7.b illustrate the behavior of the one dimensional off-shell matrix elements $\langle\chi_{k'_z} \mid v(\mathbf{Q}=0,z) \mid \chi_{k_z}\rangle$ and $\langle\chi_{k'_z} \mid -(\partial/\partial z)v(\mathbf{Q}=0,z) \mid \chi_{k_z}\rangle$ which determine the parallel and perpendicular components of expression (12), respectively. The minima occurring in these plots are the consequence of the competition between the contributions coming from the repulsive and attractive components of $v(\mathbf{Q}=0,z)$.

As is clear from Eq. (11), the calculations of the full interaction matrix elements also require the dynamical displacements $\mathbf{u_l}$ of atoms in the adlayer. For Xe adsorption on Cu(001) the overlayer structure is incommensurate with the underlying substrate which necessitates an approximate but consistent description of the adlayer vibrational properties. Following the experimental evidence indicating a defect free and well structured monolayer (c.f. Fig. 2) we assume as in Sec. III a planar "floating adlayer" with perfect hexagonal symmetry in which the phonon dynamics takes into account only the averaged Xe-substrate potential perpendicular to the surface as well as inter-adsorbate interactions. In this case the polarization vectors and eigenfrequencies are solutions of a three-dimensional dynamical matrix [24]. Hence, the adsorbate displacements can be expanded in terms of normal phonon modes of the adlayer in terms of phonon creation ($a^\dagger_{\mathbf{Q},j}$) and annihilation ($a_{\mathbf{Q},j}$) operators:

$$\mathbf{u_l} = \sum_{\mathbf{Q},j}\left(\frac{\hbar}{2M_aN_a\omega_{\mathbf{Q},j}}\right)^{1/2} e^{i\mathbf{Q}\boldsymbol{\rho}_\mathbf{l}}\mathbf{e}(\mathbf{Q},j)(a_{\mathbf{Q},j}+a^\dagger_{-\mathbf{Q},j}), \tag{15}$$

which also defines $\mathbf{u}(\mathbf{Q},j) = (\hbar/2M_aN_a\omega_{\mathbf{Q},j})^{1/2}\mathbf{e}(\mathbf{Q},j)$ in Eq. (11). Here $\boldsymbol{\rho}_\mathbf{l}$ is the parallel component of the radius vector of the **l**-th adsorbate in equilibrium, and M_a and N_a are the mass and the number of Xe atoms in the adlayer, respectively. In the floating adlayer model the index j ranges over the S- (shear vertical), L- (longitudinal horizontal) and SH-

(shear horizontal) adlayer modes. By construction the floating adlayer phonon modes are localized in the adlayer and the polarizations of L- and SH-modes are strictly in the surface plane. The corresponding dispersion curves calculated with the adjusted force constants quoted in Sec. III are shown in Fig. 8. Consequently, the symmetry selection rules for probability of phonon excitation in a floating adlayer are more stringent than in the case of a dynamical matrix description which includes the substrate dynamics in some way. This is reflected in the calculated probability of excitation of an SH-phonon for in-the-sagittal plane inelastic scattering within the first SBZ of the superstructure. This probability turns out to be much smaller than for the L-mode for all azimuths, and is exactly zero along the two high symmetry directions $\Gamma\bar{K}_{Xe}$ and $\Gamma\bar{M}_{Xe}$ of the superstructure. These effects will be further discussed below in conjunction with the effects which the scattering potential imparts to the scattering intensities and in Sec. V where we discuss a comparison between experimental and theoretical results.

To calculate the required eigenfrequencies and the corresponding polarization vectors of the full dynamical matrix corresponding to the commensurate Xe/Cu(111) system we have used the force constants given in the previous section. The results for the dispersion curves are shown in Fig. 9.a. Here we can also trace how each phonon mode of the composite system is localized at the surface (i.e. within the adlayer) and how typical surface modes may get delocalized for certain values of the wave vector. A measure of the adlayer localization of the S-, L- and SH-modes near the center of the first BZ of the superstructure is shown in Fig. 9.b. Further important information concerning the ellipticity of polarization (perpendicular versus longitudinal) of the L-mode in the same region is illustrated in Fig. 9.c.

The calculation of the force matrix elements, Eq. (12), can be performed analytically [61] using the wave functions of Eq. (3) and the two dimensional Fourier transform of the pair interaction, Eq. (13) [58]. With the aid of these matrix elements and using Eqs. (7) and (8), we can obtain first order or distorted wave Born approximation (DWBA) transition probabilities for He atoms in Eq. (6). Multiplying them by the corresponding Bose distributions we obtain the DWBA inelastic state-to-state reflection coefficients for one phonon scattering

[31]. Carrying out the summation over k'_z by making use of Eq. (8), fixing $\theta_{SD} = \theta_i + \theta_f$, E_i and T_s, and varying θ_i we obtain the Q-dependent scattering intensities which can be directly related to the one phonon intensities in the TOF spectra (c.f. next section). Here we shall only illustrate some of their general and most interesting features.

Figure 10 shows a plot of the DWBA scattering intensities for emission (energy loss) or absorption (energy gain) of a single dispersionless S-phonon in HAS from the "floating" Xe adlayer on Cu(001) surface. The calculated intensities reveal a relatively simple and expected structure as a function of the exchanged phonon momentum which is mainly due to simple properties of S-phonons characteristic of the "floating" adlayer model (absence of dispersion and the polarization vector localized in and perpendicular to the adlayer). On the other hand, due to the more complicated model of vibrational dynamics of the commensurate Xe monolayer adsorbed on Cu(111) surface the analogous intensities shown in Fig. 10.b exhibit a more complicated structure despite the similarity in the corresponding potential parameters (for the magnitude of the latter see next section). Here the S-phonon polarization vector becomes delocalized over the first few layers of the Xe/Cu slab for the values of Q at which the S-phonon dispersion curve meets the dispersion curves of substrate phonons (c.f. Fig. 9.a). This makes the coupling of the He atom to S-phonons weaker in this region of the Q-space which is then reflected in the occurrence of pronounced minima in the scattering intensities.

However, for nondispersive S-phonons the intensities of the measured single quantum loss or gain peaks acquire additional weight due to the multi-quantum interference between the emission of $n \pm 1$ and annihilation of n nondispersive phonons of different wave vectors [62,63]. These additional contributions are automatically included in the EBA with account of recoil effects, as demonstrated in Ref. [64]. The difference between the single S-phonon loss and gain scattering intensities obtained in first order DWBA theory and in the EBA (which takes into account such interference processes) can also be visualized in Figs. 10.a and 10.b for incommensurate and commensurate Xe adlayers, respectively. It is seen from the figures that for given projectile incoming energies these differences may be already quite

substantial. In particular, the noticeably larger EBA intensities for larger wave vectors are solely due to multi-quantum interference processes. This necessitates the use of the EBA in calculating the scattering intensities for comparison with the experimental data. On the other hand, we have found that the same type of renormalization of the scattering intensities of dispersive L-modes by emission and absorption of nondispersive S-modes gives a negligible effect.

The differences in magnitude between the projectile transition probabilities in one phonon loss and gain processes can be best illustrated by repeating the above calculation for the scattering intensities but without multiplying the phonon loss and gain transition probabilities by the corresponding Bose distributions. The results of such a calculation for an S-mode emission and absorption are depicted in the insets in Figs. 10.a and 10.b. These differences arise from and give a measure of the quantum recoil effects and are more pronounced at lower projectile incoming energies (c.f. Fig. (6) in Ref. [19]). The trend that the results for loss processes give smaller values than for the gain processes reflects the fact that the phase space or density of states for transitions of the projectile to a state with lower energy (case of phonon emission) is smaller than to a state with higher energy (case of phonon absorption).

Figure 11.a shows first order or DWBA intensities for HAS from L-phonons in the incommensurate adlayer of Xe on Cu(001) surface for finite substrate temperature T_s which determines the temperature of the Bose-Einstein distributions for adlayer phonons in expression (6). In the present "floating" adlayer model for the dynamical matrix the L-mode frequency follows acoustic dispersion $\omega_{\mathbf{Q},L} \propto c_L Q$ for small Q (c.f. Fig. 8). The corresponding polarization vector $\mathbf{e}(\mathbf{Q}, L)$ lies strictly in the adlayer plane and remains dominantly parallel to $\mathbf{Q}$ even outside the high symmetry directions of the BZ of the superstructure. Consequently, the L-phonon DWBA intensity for small Q (for which $\omega_{\mathbf{Q},L} \propto Q$) and finite T_s becomes proportional to the factor $\mid \mathbf{Q} \cdot \mathbf{e}(\mathbf{Q}, L) \mid^2 kT_s/\omega^2_{\mathbf{Q},L}$ which saturates at a finite value for $Q \to 0$. As a result of that and the properties of the matrix elements depicted in Fig. 7.a the L-phonon scattering intensity in the case of the incommensurate monolayer exhibits a maximum near the zone center. The minima in the intensity occur for those val-

ues of Q at which the on-the-energy-shell counterparts of these matrix elements go through a minimum or zero. All these features clearly manifest themselves in the Q-dependence of the L-phonon scattering intensity shown in Fig. 11.a. In contrast to the L-mode behavior, the polarization of the SH-mode remains dominantly perpendicular to $\mathbf{Q}$ also outside the high symmetry directions of the first SBZ of the superstructure [37]. Therefore for ideally structured "floating" adlayers it will always give a much smaller contribution to the intensity of the one phonon processes for HAS in the sagittal plane and $\mathbf{Q}$ restricted to the first SBZ (c.f. next section).

Figure 11.b shows the single L-phonon HAS intensity for Xe/Cu(111) system as a function of the phonon wave vector on the same scale as in Fig. 11.a. Apart from the trends leading to zero scattering intensities for some isolated Q-values due to the behavior of the off-shell matrix elements shown in Fig. 7.a, which are common to both incommensurate and commensurate Xe layers, some basic differences with respect to the Xe/Cu(001) system can be observed. The commensurability of the adlayer with the substrate gives rise to non-vanishing Xe-Cu shear stress force constants entering the full dynamical matrix of the Xe/Cu slab, thereby producing two important effects regarding the phonon dynamics. First, it causes the appearance of a zone center phonon gap in the dispersion curves of L-phonons and hence the intensity factor $\mid \mathbf{Q}\cdot\mathbf{e}(\mathbf{Q},L) \mid^2 kT_s/\omega^2_{\mathbf{Q},L} \propto Q^2$ for small Q because $\omega_{\mathbf{Q}=0,L} \neq 0$. Second, the polarization vector of the L-phonons is no longer constrained to the surface plane but for the values of Q at which the L-mode and substrate modes are degenerate it also acquires a component in the direction perpendicular to the surface and its localization to the adlayer is reduced (c.f. Figs. 9.b and 9.c). For a completely in-surface-plane polarization of the L-mode and finite T_s the first effect causes a drop in the scattering intensity which is quadratic in Q towards the zone center. The beginning of this trend is clearly visible in Fig. 11.b. However, by increasing Q the second effect begins to play a role and, since the coupling to perpendicular vibrations is much stronger than to the parallel ones, the L-phonon scattering intensity rises rapidly up and reaches a maximum in two spikes near the zone center. Hence, the interplay between the parallel and perpendicular polarizations, or the

ellipticity of the L-mode polarization in the commensurate Xe/Cu(111) system, introduces fast variations of the scattering intensity as a function of the exchanged phonon momentum. Regarding the role of the SH-modes of the slab on the HAS intensities, we find that the situation here is completely analogous to the case of a floating Xe adlayer, i.e. within the present model description their coupling to He atom is generally negligible for in-sagittal-plane collision geometry and $\mathbf{Q}$ lying in the first SBZ, and is strictly zero along the high symmetry directions. However, this conclusion does not apply to the magnitude of the Debye-Waller factor because the Debye-Waller exponent is obtained by carrying out the momentum transfer summations over the entire first SBZ and also beyond if the coupling matrix elements are strong there (c.f. Figs. 10 and 11). In fact, for the matrix elements of appreciable magnitude in the second SBZ the SH-mode can produce even larger contributions to the DW exponent than the L-mode due to its lower excitation frequency. This situation is illustrated in Fig. 12.

An important point to be observed in connection with Figs. 10 and 11 is a relatively large difference between the one phonon loss and gain scattering probabilities at lower projectile incident energies. This is due to an interplay between the projectile recoil and temperature effects. The amplitude for a transition of the projectile to a state with higher energy is larger than to a state with lower energy (c.f. insets in Figs. 10.a and 10.b) because of the larger phase space for the states of higher energy. Thus, for the same incoming energy the matrix elements $\mid \mathcal{V}(-) \mid^2$ for phonon absorption in expression (6) for the scattering function will be generally larger than $\mid \mathcal{V}(+) \mid^2$ which describe phonon emission (c.f. also Fig. 6 in Ref. [19]). On the other hand, the temperature effects entering expression (6) through the corresponding Bose-Einstein distribution factors $\bar{n}$ and $(\bar{n}+1)$ for phonon absorption and emission, respectively, act just in the opposite direction because $\bar{n} < (\bar{n}+1)$. Hence, the total scattering intensity for phonon emission or absorption calculated from the scattering function (6) depends on the trade off between these two effects.

V. COMPARISON OF THEORETICAL AND EXPERIMENTAL RESULTS

A real test of the assumptions underlying the present model interpretation of HAS from Xe monolayers on Cu(001) and Cu(111) surfaces should come through a comparison of relative excitation intensities of the various modes in the experimental and calculated scattering spectra. This is equally relevant for the single and multiphonon scattering regimes.

In this section we first calculate the relative intensities of the various adlayer modes in the single phonon scattering regime using the approaches described in the preceding sections. The parameters characterizing the He-Xe potential in expression (13) are given by:

$D = 6.60$ meV, $\alpha^{-1} = 0.8202$ Å, and $z_0 = 3.49$ Å,

for the commensurate system Xe/Cu(111), and

$D = 6.40$ meV, $\alpha^{-1} = 1.032$ Å, and $z_0 = 3.6$ Å,

for the incommensurate system Xe/Cu(001). These are not the parameters obtained from pairwise summation of pure He-Xe gas-phase potentials [56] which yields:

$D_{gas} = 7.2$ meV, $\alpha_{gas}^{-1} = 0.77$ Å, and $z_{0,gas} = 3.51$ Å,

but slightly modified ones to produce a softer He-surface potential. The present set of parameters for the Xe/Cu(111) system also differs from the one quoted in Ref. [10] which is a result of additional consistency requirement imposed to obtain a unified set describing the TOF spectral intensities equally well in the single and multiphonon scattering regimes. Such a necessity for modification of the sum of gas-phase pair potentials is not uncommon in HAS studies (c.f. Refs. [60,65]) and here it is also necessary to consistently reproduce the relative peak intensities in the measured TOF spectra.

A comparison of the experimental and calculated spectral intensities of S- and L-modes in the single phonon scattering regime of HAS from Xe/Cu(111) is shown in Fig. 13. Here we note that our calculations always yield smaller intensities for the elastic peaks compared with the experiment as the latter also includes contributions from diffuse elastic scattering from defects not accounted for by the present model. Hence, this missing component has been added to the elastic peak intensity because in combination with the finite peak width

it can also contribute to the background intensity of the L-peaks. With this proviso a good agreement between experimental and theoretical results is achieved which illustrates the consistency of the present interpretation of the inelastic peaks in the TOF spectra.

Since in the floating adlayer model applied to the Xe/Cu(001) system the interference between the adlayer modes and the substrate Rayleigh wave (RW) cannot be obtained, we have selected the TOF spectra in which the peaks assigned to S- and L-modes could be maximally separated from those of the RW and then calculated only the adlayer mode intensities in the EBA by neglecting the S-mode frequency shifts and delocalization occurring at avoided crossing with the dispersion curve of the RW. Along the direction of measurement the polarization of the SH mode is not strictly perpendicular to its wave vector, and this in principle could give rise also to SH-mode-induced structures in the TOF spectra. However, in this direction the present theoretical analysis gives the SH-mode intensity of the order of only five percent relative to the contribution from the L-mode. Only the introduction of coupling of the SH mode to the modes of the underlying substrate could induce a breakdown of symmetry leading to a removal of such stringent selection rules and thereby to a larger SH-mode excitation probability. The calculated relative intensities of the S- and L-modes for the Xe/Cu(001) system in the single phonon scattering regime, but with inclusion of multi-quantum interference of nondispersive S-modes, are compared with the experimental data in Fig. 14. Given all the approximations used in the calculation, it is seen that the model reproduces the relative TOF intensities quite satisfactory. The only exception occurs on the energy loss side in the lower panel of Fig. 14 where the afore mentioned avoided crossing between the substrate RW (energy loss at 3.05 meV) and the adlayer S-mode takes place, with the effect of S-mode frequency shift and intensity enhancement. In Fig. 14 we also demonstrate how the use of the unsoftened force constants derived from the three-dimensional Xe-Xe gas phase potential [13] produces the position and intensity of L-peaks for which the disagreement with the experimental data is evident. On the other hand, the SH-peaks calculated for the present scattering geometry by using the same gas phase potentials are of negligible relative intensity to be experimentally observable although their

frequency may coincide with that of the measured acoustic mode. Hence, with the present mode assignments and the corresponding model dispersion relations based on the softened radial intralayer force constants we can consistently describe the HAS-TOF intensities for the Xe/Cu(001) system as well.

As the coupling of He atoms to S-modes is much stronger than to the L-modes, as illustrated in Figs. 10 and 11, the multiphonon scattering spectra will be dominated by a series of multi-quantum S-peaks. All other dispersive modes may only add weak structures on top of this basic one. Eventually, these structures will turn into a broad Gaussian-like background (cf. Eq. (73) in Ref. [15] and Eq. (9) and Fig. 3 in Ref. [16]) in the limit of high incident projectile energies. The multiphonon scattering spectra from Xe/Cu(111) and Xe/Cu(001) adlayers have been studied in detail in Ref. [19] and for the sake of completeness we here briefly illustrate their features in Figs. 15.a and 15.b, respectively, by consistently employing the potentials from the corresponding single phonon calculations. Figure 15.b is interesting in that it illustrates the behavior of the experimental scattering spectra of He→Xe/Cu(001) collisions in the single phonon scattering regime regarding the modes which weakly couple to He atoms. This is shown by the appearance of a Rayleigh wave-induced hump and an L-mode-induced shoulder near the elastic line. However, this scattering regime simultaneously appears to be a multiphonon one for the S-modes whose coupling to the scattering He atoms is much stronger. Concerning the agreement between experimental and theoretical results we observe that although the multiphonon TOF spectra of the incommensurate Xe/Cu(001) system can be relatively well reproduced, except for the elastic line which was not corrected for diffuse scattering contribution in the theoretical plot, the agreement for the commensurate Xe/Cu(111) system is better. Interestingly enough, in the latter case (Fig. 15.a) the diffuse elastic scattering correction for the elastic line was unnecessary due to the true multiphonon character of the spectrum at this higher incident energy. This spectrum can be viewed as a convolution of a series of well defined equidistant peaks, signifying the uncorrelated multiple emission and absorption of nondispersive S-phonons and not the overtones (for overtone frequencies see next section), with a broad

background arising from the multiple excitation of L- and SH-phonons (whose polarizations in this regime are no more constrained by the symmetry selection rules), and also from the substrate surface projected modes which may couple to the scattered He atoms. As implied in expression (6), the phonon absorption processes of any kind can take place only for $T_s > 0$.

It is also noteworthy that the resulting multi-quantum S-mode intensities in the spectra shown in Figs. 15.a and 15.b do not generally follow the Poisson distribution. This arises as a consequence of the projectile recoil effects and the dependence of the magnitude of each peak maximum on the exchanged parallel momentum, which both act so as to prevent the appearance of a simple Poissonian structure. These features were discussed in detail in Refs. [19,64,66].

VI. CORRUGATION OF Xe-Cu(111) POTENTIAL ENERGY SURFACE

The value of the zone center gap for the longitudinal phonon mode in the case of Xe adsorbed on Cu(111) surface also provides information on the Xe/Cu(111) potential energy surface. Since, in the past, precise information on the lateral corrugation for noble gases adsorbed on metal surfaces has been missing, an approach based on the work by Steele [67] has frequently been used in applications [68] in which the periodic adsorbate-substrate potential $V_s(\mathbf{r})$ is obtained by a summation of Lennard-Jones pair potentials $V(\mathbf{r}) = 4\epsilon[(\sigma/r)^{12} - (\sigma/r)^6]$ describing interaction between noble gas atom and substrate atoms. The resulting sum can be expressed in the form

$$V_s(\boldsymbol{\rho}, z) = \epsilon[V_0(z) + f\, V_1(z) \sum_{i=1}^{3} \cos(\mathbf{G}_i \cdot \boldsymbol{\rho})]. \tag{16}$$

where now $\boldsymbol{\rho}$ and z denote the adsorbate parallel and perpendicular coordinate, respectively, the latter being measured from the first layer of substrate atoms. The symbols $\pm\mathbf{G}_i$, $i = 1$ to 3, denote the six shortest reciprocal lattice vectors, and the definition of V_0 and V_1 is given in Ref. [67]. The original expression (16) was derived in Ref. [67] for the case $f = 1$ and the extra factor f which may differ from unity has been added following Ref. [68] to adjust

the corrugation without changing the adsorption energy. Since this type of the potential has been used in molecular dynamics simulations of sliding monolayers we can estimate its relevance to the present problem even without invoking the precise information on the adsorption sites. Thus, setting σ to 3.487 Å, the arithmetic mean of σ_{Xe-Xe} (describing the Xe-Xe interaction), the Cu nearest neighbor distance [69] and putting $\epsilon = 19$ meV, yields a Xe-surface potential with a total depth of around 200 meV, a reasonable value [27]. For the interaction between noble gas atoms and metal surfaces with highly delocalized conduction electrons the parameter f has previously been reduced to values of the order 0.1 to account for small corrugations observed experimentally, and values as small as 0.03 have been proposed for the case of Kr on Au(111) [68].

Although we have not used the parametrized expression (16) in our dynamical matrix analysis of Xe adlayer vibrations, we would like to point out that for the potential parameters appropriate to Xe on Cu(111) (see above) a value of $f = 0.1$ yields a zone center phonon gap energy of 0.25 meV, significantly smaller than the value reported here. In addition, using this potential energy surface (PES) the computed S-phonon energy amounts to 4.55 meV (i.e. much larger than the present experimental value $\hbar\omega_S = 2.62$ meV), and the anharmonic shift of the fifth overtone to ∼0.5 meV. The same conclusion can be also derived by using the Xe-Cu(111) potentials parametrized in Refs. [27,28]. To get the correct curvature of the PES at the adsorption site one should either change by a substantial amount the depth of the potential (16) in the normal direction (governed by ϵ), or modify its width which is controlled by σ, or both. Drastic changes in the potential depth leading to the experimental vibrational energies are physically implausible in view of the correct fitting of the desorption energies. On the other hand, the correct curvature can be achieved by a modest, 10% softening of the repulsive component of the potential. This is consistent with the softening of the L-mode force constants discussed in Sec. III and the modification (also in the direction of softening) of the He-Xe adlayer potential noted in Sec. V. All three features, which derive from independent analyses of the experimental data, unambiguously point towards the effect of softening of pair interactions involving Xe atoms in adsorbed monolayer phase.

In the previous report of the present results for Xe/Cu(111) [10] an incorrect reference was made to the work of Cieplak, Smith and Robbins [68] in which the results of molecular dynamics simulations for Kr adsorbed on Au(111), i.e. not Xe on Ag(111), were reported. Considering the analysis presented in the last paragraph, we believe that the PES used in that work [68] may be too weakly corrugated when the factor f is reduced to below the value of 0.1. Since the molecular dynamics results on friction of sliding noble gas adlayers show a pronounced dependence on the strength of lateral corrugation [68,70] it would be highly desirable to experimentally determine the zone center gap of the longitudinally polarized phonon modes of Kr and Xe adsorbed on Ag(111) or Au(111). Unfortunately, however, such measurements are hampered by the fact that on these substrates both noble gases form incommensurate overlayers in which the zone center phonon gap is zero because of the translational invariance.

VII. SUMMARY AND CONCLUSIONS

In this work we have carried out a comprehensive comparative experimental and theoretical study of low energy dynamics of monolayers Xe on Cu(111) and Cu(001) surfaces by utilizing the HAS-TOF spectroscopy and a recently developed quantum theory of inelastic HAS from surfaces which treats single and multiphonon scattering processes on an equivalent footing. The inelastic HAS data were obtained for a wide range of initial scattering conditions (E_i, θ_i, T_s) spanning the single and multiphonon scattering regimes. The data have been carefully analyzed by combining the dynamical matrix approach for description of the adlayer vibrational dynamics with the developed scattering theory.

For both substrates the angular distributions (diffraction spectra) of scattered He atoms signified hexagonally ordered Xe monolayers, the commensurate $(\sqrt{3} \times \sqrt{3})\mathrm{R}30^0$ adlayer in the case of the Cu(111) surface [20,21] and the incommensurate one in the case of the Cu(001) surface [22,23]. The measured phonon dispersion relations deduced from the TOF spectra for the two types of monolayers exhibited great similarities in the case of the nondispersive

optical-like S-phonons localized in the adlayer. However, a striking difference occurred in the case of the very soft dispersive phonon branch labeled "L". In the incommensurate phase it is genuinely acoustic-like whereas in the commensurate phase it exhibits a frequency band gap at the zone center.

The tentative mode assignment was first made by employing the symmetry selection rules applicable to one-phonon excitation processes in HAS in the sagittal plane in combination with the dynamical matrix description of the adlayer vibrational modes. Since in the case of the Xe/Cu(001) system no signature of a possible high order commensurate phase has been found, the dynamical matrix treatment of the two adlayers was markedly different. On Cu(001) it was only possible to treat incommensurate Xe adlayer as an ideally structured hexagonal monolayer floating on a structureless substrate surface with adlayer modes completely decoupled from those of the substrate. On the other hand, for the monolayer of Xe on Cu(111) it was possible to construct a full dynamical matrix of the vibrationally coupled Xe/Cu(111) system. Despite these differences it was possible to establish a unified model interpretation of the observed modes in both systems in terms of a consistent set of adjusted Xe-Xe and Xe-Cu force constants. In this picture the S-mode is dominantly adlayer localized and FT_z or vertically polarized. In order to reconcile the symmetry selection rules for excitation of in-plane-polarized adlayer-induced modes in HAS from ideally structured adlayers with the dynamical matrix description of the modes, we had to assign a dominantly longitudinal polarization to the "L"-mode (L-phonon), with a possibility of a relatively strong vertical or z-admixture (up to $\sim 15\%$) near the avoided crossings with other surface projected modes. By consistently carrying out this procedure we found that the radial Xe-Xe force constants determining the dispersion of the thus assigned longitudinal modes turned out much softer than by directly applying the sophisticated HFD-B2 Xe-Xe gas phase pair potential [13]. Such a modification of the interadsorbate interactions still awaits its interpretation through a detailed calculation of the electronic structure of Xe adlayers on Cu(111) and Cu(001). The magnitude of the band gap in the dispersion of L-phonons in the commensurate Xe/Cu(111) phase was used to obtain information on the

corrugation of the Xe atom-substrate potential in this system [10].

The assignment of the observed acoustic modes to shear horizontal or SH-modes in the first SBZ, which were the subject of recent controversy [12], was ruled out for both systems first by invoking the symmetry selection rules (c.f. Sec. III) for the excitation of the various in-plane modes in HAS. Following these arguments, in the present model in which the ideal structure of Xe adlayers is an essential ingredient, the SH-mode can give only a negligible contribution to the scattering intensity relative to the longitudinal mode.

These interpretations were then corroborated by detailed theoretical analyses of the scattering intensities in the HAS-TOF spectra. We have first analyzed and demonstrated the difference between the interaction matrix elements coupling the scattering He atoms to the perpendicular and parallel to the surface vibrations of the adlayer for small parallel momentum transfer and variable incoming projectile energy. Combining this with the calculated properties of the polarization vectors of the adlayer modes, we were able to obtain the one-phonon HAS intensities of the adlayer modes and compare them with experiments. A good and consistent agreement between experimental and model theoretical results for the S- and L-modes was obtained in all aspects of the measured data for both types of Xe adlayers.

The theory was then extended to calculations of the scattering spectra in the transition from the single to the truly multiphonon scattering regime which is characterized by the value of the corresponding Debye-Waller exponent larger than unity. Interestingly enough, for the S-modes, which strongly couple to the scattered He atoms, the multiphonon regime is already reached for the scattering conditions which still favor the single L-phonon scattering. The interplay of these two types of couplings gives rise to the characteristic spectral shapes of the multiphonon HAS TOF spectra. A very good agreement between the calculated results and the TOF data in this regime gives further support to our earlier assignments, the consistency of the model description of the low energy dynamics of the two distinct monolayer phases of Xe, and the adequacy of the present treatment of single and multiphonon He atom scattering from these adlayers.

ACKNOWLEDGMENTS

The work in Zagreb has been supported in part by the National Science Foundation grant JF-133, and the work in Bochum in part by the German DFG grant Wo 464/14-1.

REFERENCES

[1] D.M. Eigler and E.K. Schweizer, Nature (London) **344**,524(1990).

[2] G. Meyer, L. Bartels, S. Zöphel, E. Henze and K.-H. Rieder, Phys. Rev. Lett. **78**,1512(1997).

[3] See articles in: *Physics of Sliding Friction*, edited by B.N.J. Persson and E. Tosatti, Kluwer Academic Publishers, Dordrecht/Boston/London, 1996.

[4] G. Witte, K. Weiss, P. Jakob, J. Braun, K.L. Kostov and Ch. Wöll, Phys. Rev. Lett. **80**,121(1998).

[5] See for example: W. Widdra, P. Trischberger, W. Friess, D. Menzel, S.H. Payne and H.J. Kreuzer, Phys. Rev. **B57**,4111(1998); and references therein.

[6] B.F. Mason and B.R. Williams, Phys. Rev. Lett. **46**,1138(1981).

[7] K. D. Gibson, S. J. Sibener, B. Hall, D. L. Mills, and J. E. Black, J. Chem. Phys. **83**,4256(1985).

[8] P. Zeppenfeld, M. Büchel, R. David, G. Comsa, C. Ramseyer and C. Giradet, Phys. Rev. **B50**,14667(1994).

[9] A.P. Graham, M.F. Bertino, F. Hofmann, J.P. Toennies and Ch. Wöll, J. Chem. Phys. **106**,6194(1997).

[10] J. Braun, D. Fuhrmann, A. Šiber, B. Gumhalter and Ch. Wöll, Phys. Rev. Lett. **80**,125(1998).

[11] R. Gerlach, A.P. Graham, J.P. Toennies and H. Weiss, J. Cem. Phys. **109**,5319(1998).

[12] L.W. Bruch, J. Chem. Phys. **107**,4443(1997); A.P. Graham, M.F. Bertino, F. Hofmann, J.P. Toennies, and Ch. Wöll, J. Chem. Phys. **107**,4445(1997); L.W. Bruch, preprint (MPI für Strömungsforschung, Göttingen, 1997).

[13] A.K. Dham, W.J. Meath, A.R. Allnatt, R.A. Aziz, and M.J. Slaman, Chem. Phys. **142**,173(1990).

[14] M.T. Dove, *Introduction to Lattice Dynamics* (Cambridge University Press, Cambridge, 1993).

[15] A. Bilić and B. Gumhalter, Phys. Rev. **B 52**,12307(1995).

[16] B. Gumhalter and A. Bilić, Surf. Sci. **370**,47(1997).

[17] B.J. Hinch, A. Lock, H.H. Madden, J.P. Toennies and G. Witte, Phys. Rev. **B 42**,1547(1990).

[18] J. Jupille, J.-J. Erhardt, D. Fargues and A. Cassuto, Faraday Discuss. Chem. Soc. **89**,323(1990); Vacuum **41**/No. 1-3,399(1990).

[19] J. Braun, D. Fuhrmann, M. Bertino, A.P. Graham, J.P. Toennies, Ch. Wöll, A. Bilić and B. Gumhalter, J. Chem. Phys. **106**,9922(1997).

[20] M.A. Chesters, M. Hussain and J. Pritchard, Surf. Sci. **35**,161(1973).

[21] Th. Seyller, M. Caragiu, R.D. Diehl, P. Kaukasoina and M. Lindroos, Chem. Phys. Lett. **291**,567(1998).

[22] M.A. Chesters and J. Pritchard, Surf. Sci. **28**,460(1971).

[23] A. Glachant and U. Bardi, Surf. Sci. **87**,187(1979).

[24] Ch. Wöll, Appl. Phys. **A53**,377(1991).

[25] U. Harten, J.P. Toennies and Ch. Wöll, Faraday Discuss. Chem. Soc. **80**,137(1985).

[26] B. Hall, D. L. Mills, P. Zeppenfeld, K. Kern, U. Becher and G. Comsa, Phys. Rev. **B40**,6326(1989).

[27] A. Chizmeshya and E. Zaremba, Surf. Sci. **268**,432(1992).

[28] G. Vidali, G. Ihm, H.-Y. Kim, M.W. Cole, Surf. Sci. Rep. **12**,133(1991).

[29] G. Benedek, J. Ellis, N.S. Luo, A. Reichmuth, P. Ruggerone and J.P. Toennies Phys. Rev. **B48**,4917(1993); C. Kaden, P. Ruggerone, J.P. Toennies, G. Zhang and G. Benedek, Phys. Rev. **B46**,13509(1992).

[30] R. E. Allen, G. P. Alldredge, and F. W. de Wette, Phys. Rev. **B4**, 1648 (1971).

[31] V. Celli in *Surface Phonons*, editors W. Kress and F.W. de Wette (Springer, Berlin 1991), p.167.

[32] G. Santoro and V. Bortolani in *Inelastic Energy Transfer in Interactions with Surfaces and Adsorbates*, edited by B. Gumhalter, A.C. Levi and F. Flores (World Scientific, Singapore, 1993), p. 1.

[33] A. Glebov, W. Silvestri, J.P. Toennies, G. Benedek and J.G. Skofronick, Phys. Rev. **B54**,17866(1996).

[34] N.D. Lang, Phys. Rev. Lett. **46**,842(1981); N.D. Lang and A. R. Williams, Phys. Rev. **B25**,2940(1982).

[35] B. Hall, D.L. Mills and J.E. Black, Phys. Rev. **B 32**,4932(1985).

[36] J. Ellis, J.P. Toennies and G. Witte, J. Chem. Phys. **102**,5059(1995).

[37] B. Gumhalter, unpublished.

[38] M. Wolf, E. Knoesel and T. Hertel, Phys. Rev. **B54**,R5295(1996).

[39] K. Burke, B. Gumhalter and D.C. Langreth, Phys. Rev. **B47**,12852(1993-I).

[40] B. Gumhalter, K. Burke and D.C. Langreth, Surf. Rev. Lett., **1**,133(1994).

[41] J. Braun, D. Fuhrmann, J.P. Toennies, Ch. Wöll, A. Bilić and B. Gumhalter, Surf. Sci. **368**,232(1996).

[42] V. Celli, D. Himes, P. Tran, J.P. Toennies, Ch. Wöll and G. Zhang, Phys. Rev. Lett.

66,3160(1991).

[43] J.R. Manson, V. Celli and D. Himes, Phys. Rev. **B49**,2782(1994); J.R. Manson, Comput. Phys. Communications **80**,145(1994).

[44] V. Bortolani and A.C. Levi, La Rivista del Nuovo Cimento **9**/No. 11,1(1986).

[45] V. Bortolani, A. Franchini, G. Santoro, J.P. Toennies, Ch. Wöll and G. Zhang, Phys. Rev. **B40**,3524(1989).

[46] G. Witte, J.P. Toennies and Ch. Wöll, Surf. Sci. **323**,228(1995).

[47] W. Brenig, Z. Physik **B 36**,81(1979).

[48] H.-D. Meyer, Surf. Sci. **104**,117(1981).

[49] R. Brako, Surf. Sci. **123**,439(1982).

[50] K. Kern, P. Zeppenfeld, R. David and G. Comsa, J. Electron Spec. Rel. Phen. **44**,215(1987).

[51] B. Gumhalter, Surf. Sci. **347**,237(1996).

[52] It has been shown that an approximate expression similar to (5) can be obtained also for the probability of electron scattering by optical surface phonons (see E. Evans and D.L. Mills, Phys. Rev. **B7**,853(1973)). The validity of such expression has been demonstrated in a passage from quantum-mechanical to quasiclassical description of the projectile motion assuming long range projectile-phonon interaction.

[53] (a): J.R. Manson and G. Armand, Surf. Sci. **184**,511(1987); (b): ibid. Surf. Sci. **195**,513(1988).

[54] V. Celli, G. Benedek, U. Harten, J.P. Toennies, R.B. Doak and V. Bortolani, Surf. Sci. **143**,L376(1984).

[55] K.T. Tang and J.P. Toennies, Z. Phys. **D1**,91(1986).

[56] U. Kleinekathöfer, K.T. Tang, J.P. Toennies and C.L. Yiu, Chem. Phys. Lett. **249**,257(1996); U. Kleinekathöfer, Ph.D. thesis, University Göttingen, 1996; Max-Planck-Institut für Strömungsforschung Bericht 6/1996.

[57] G. Gašparović, B.Sci. thesis, University of Zagreb, 1997 (unpublished).

[58] A. Šiber and B. Gumhalter, Surf. Sci. **385**,270(1997).

[59] H. Hoinkes, H. Nahr and H. Wilsch, Surf. Sci. 33(1972)516, ibid. 40(1973)129; G. Armand, J. Lapujoulade and Y. Lejay, Surf. Sci. 63(1977)143.

[60] A. Franchini, G. Santoro, V. Bortolani, A. Bellman, D. Cvetko, L. Floreano, A. Morgante, M. Peloi, F. Tommasini and T. Zambelli, Surf. Rev. Lett. **1**,67(1994).

[61] A.F. Devonshire, Proc. Roy. Soc. **A 158**,253(1937).

[62] H. Kasai and W. Brenig, Z. Phys. **B59**,429(1985).

[63] J.R. Manson, Phys. Rev. **B37**,6750(1988).

[64] B. Gumhalter, A. Šiber and J.P. Toennies, submitted for publication.

[65] D. Eichenauer, U. Harten, J.P. Toennies and V. Celli, J. Chem. Phys. **86**,3693(1957).

[66] C.M. Hedenäs and M. Persson, Phys. Rev. **B45**,11273(1992).

[67] W.Steele, Surf. Sci. **36**, 317 (1973)

[68] M. Cieplak, E.D. Smith and M.O. Robbins, Science **265**,1209 (1994)

[69] A.D. Crowell and R.B. Steele, J. Chem. Phys. **34**,1347 (1961).

[70] B.N.J. Persson and A. Nitzan, Surf. Sci. **367**,261(1996).

FIGURES

FIG. 1. (a) Right panel: Structure of $(\sqrt{3} \times \sqrt{3})$R30° monolayer of Xe atoms (shaded circles) on (111) surface of Cu crystal, with two high symmetry directions (azimuths) in the substrate surface plane denoted. Left panel: Two dimensional Brillouin zones of the Cu(111) surface (dashed lines) and of Xe adlayer (full lines). (b) He-atom angular distribution along the $[1\bar{1}0]$ azimuth of Cu(111) from Xe $(\sqrt{3} \times \sqrt{3})$R30° monolayer for incident wave vector $k_i = 9.2$ Å^{-1} (E_i=45 meV) and surface temperature 60 K. Peaks normalized to the height of the specular peak.

FIG. 2. He-atom angular distribution along the [100] azimuth of the substrate from an incommensurate hexagonal monolayer of Xe atoms adsorbed on Cu(001) for $k_i = 5.25$ Å^{-1} ($E_i = 14.36$ meV) and substrate temperature 52 K.

FIG. 3. Series of measured HAS TOF spectra for a monolayer of Xe on Cu(111) along the $[11\bar{2}]$ direction of the substrate surface for three representative He atom incident energies. θ_i and θ_{SD} denote the angle of incidence and the fixed total scattering angle, respectively. Vertical scale measures relative peak heights in arbitrary units. Scattering parameters shown in the insets.

FIG. 4. Series of measured HAS TOF spectra for a monolayer of Xe on Cu(001) along the [100] direction of Cu surface for three representative He atom incident energies. Vertical scale in arbitrary units. Scattering parameters shown in the insets.

FIG. 5. Phonon dispersions for Xe/Cu(111) surface along the $[11\bar{2}]$ direction relative to the substrate as determined by HAS (full circles). The solid line denotes the best fit achieved for the longitudinal (L) mode in the Xe adlayer and the dashed-dotted line is the result for the L-mode using the gas phase Xe-Xe potential. The theoretical dispersion curve for the vertically polarized S-mode is marked by the long dashed line and of the Rayleigh phonon and the projected bulk phonon edge of the Cu substrate by the full thin and dotted line, respectively. For force constants see main text.

FIG. 6. Phonon dispersions for Xe/Cu(001) surface along the [100] direction relative to the Cu substrate as determined by HAS (full circles). The full curve represents the best fit achieved for the longitudinal (L) mode, the flat dashed curve shows a theoretical dispersion curve for the S-mode, the dot-dashed line indicates the position of the L-mode using the gas phase force constant. Dashed curve indicates the position of the Rayleigh wave on the Cu(001) surface. For force constants see main text.

FIG. 7. (a) Off-shell matrix elements of the potential which couples the projectile to in-plane surface vibrations (see text) for $Q = 0$ and three different values of the incoming perpendicular wave vector: $k_{zi} = 3.5$ Å(full line), $k_{zi} = 7.0$ Å(dashed line) and $k_{zi} = 14.0$ Å(dotted line), as function of scattered wave vector k'_z. Potential parameters corresponding to Xe/Cu(111) system. (b) Same for projectile coupling to perpendicular vibrations.

FIG. 8. Calculated dispersion curves of S-, L- and SH-phonons (from top to bottom) over 1/6 of the two dimensional first Brillouin zone, i.e. between two equivalent high symmetry directions, corresponding to a floating Xe adlayer on Cu(001). For force constants parametrization see main text. The angle ϕ is measured relative to $\bar{\Gamma}\bar{M}_{Xe}$ direction of the Brillouin zone of the superstructure.

FIG. 9. (a) Dispersion curves for Xe/Cu(111) system along the $[11\bar{2}]$ direction calculated using the dynamical matrix approach (see text) with Xe atoms on-top of Cu atoms. Force constants parametrization same as in Ref. [10]. Note the S-, L- and SH-mode dispersion curves detached from the bulk quasi-continuum. (b) Surface localization of Xe induced S-, L- and SH-modes on the adlayer expressed through the sum of the components of the respective polarization vectors in the adlayer. Numbers below symbols $\triangle$ denote frequencies (in meV) of the S-mode. (c) Ellipticity (vertical vs. longitudinal polarization) of the L-mode in Xe adlayer on Cu(111) substrate as function of phonon wave vector. Percentage above full squares denotes surface localization of the L-mode.

FIG. 10. (a) Calculated DWBA and EBA scattering intensities for emitting one S-phonon (lower and upper full curves, respectively, marked by (+)) and absorbing one S-phonon (lower and upper dashed curves, respectively, marked by (−)) in HAS from Xe/Cu(001) as function of exchanged phonon wave vector Q for the scattering conditions as denoted. For potential parameters see main text. Inset: Corresponding projectile transition probabilities in one phonon loss and gain processes denoted by full and dashed lines, respectively. (b) Same for Xe/Cu(111) system.

FIG. 11. (a) Calculated DWBA HAS intensity for L-phonon emission (full curve) and L-phonon absorption (dashed curve) in Xe/Cu(001) as function of exchanged phonon momentum. For interpretation of the maxima and minima see main text. (b) Same for Xe/Cu(111) system.

FIG. 12. Plots of the various contributions to the Debye-Waller factor pertinent to He→Xe/Cu(001) collision system as function of substrate temperature T_s and for the scattering conditions as denoted. Dotted line: only S-phonons included; dashed line: S- and L-phonons included; full line: S-, L- and SH-phonons included. Note the logarithmic scale on the ordinate axis. Here the $\mathbf{Q}$ summation in Eq. (6) to obtain the DW exponent was carried out over the first and second surface Brillouin zone of the superstructure.

FIG. 13. Comparison of experimental and calculated S- and L-mode intensities in the single-phonon scattering spectra typical of He→Xe/Cu(111) collisions.

FIG. 14. Comparison of experimental and calculated S- and L-mode intensities in the single-phonon scattering spectra typical of He→Xe/Cu(001) collisions. Expanded contours in the topmost panel show the positions and relative intensities of the L-mode peaks calculated with the present softened Xe-Xe radial force constants (full curve) and unmodified gas phase potential-derived [13] force constants (diamonds). Similar differences are obtained for other two spectra. SH-derived peaks not discernible on the present scale.

FIG. 15. (a) Comparison of experimental and calculated EBA multiphonon scattering spectra typical of He→Xe/Cu(111) collisions using the same potentials and dispersion relations as in Fig. 13. (b) Same for He→Xe/Cu(001) collisions using the potentials and dispersion relations as in Fig. 14.

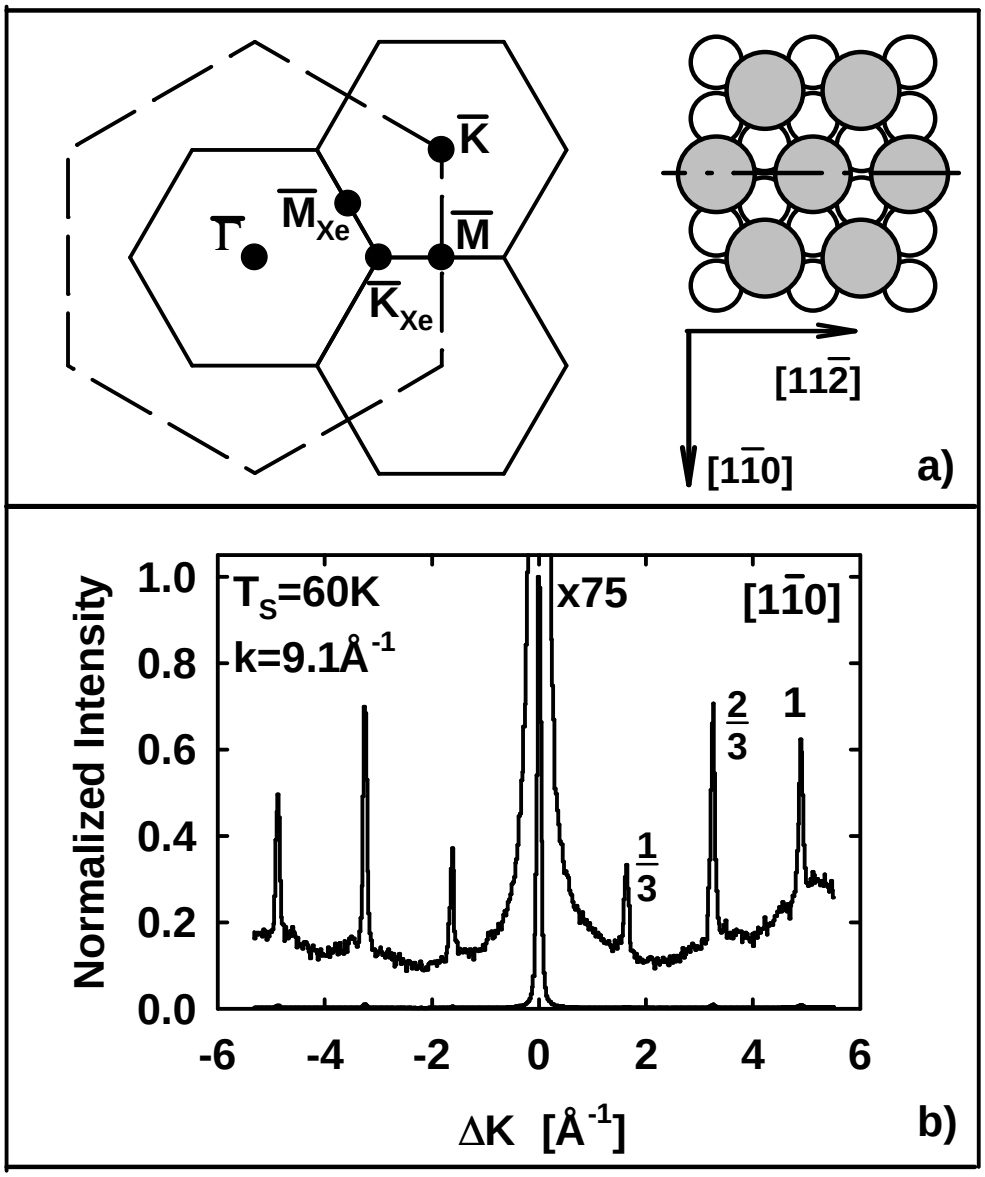
$\bar{K}$
$\bar{M}_{Xe}$
Γ
$\bar{M}$
$\bar{K}_{Xe}$
[11$\bar{2}$]
[1$\bar{1}$0]
a)
Normalized Intensity
1.0
0.8
0.6
0.4
0.2
0.0
T_S=60K
k=9.1Å^{-1}
x75
[1$\bar{1}$0]
$\frac{2}{3}$
1
$\frac{1}{3}$
-6
-4
-2
0
2
4
6
ΔK [Å^{-1}]
b)

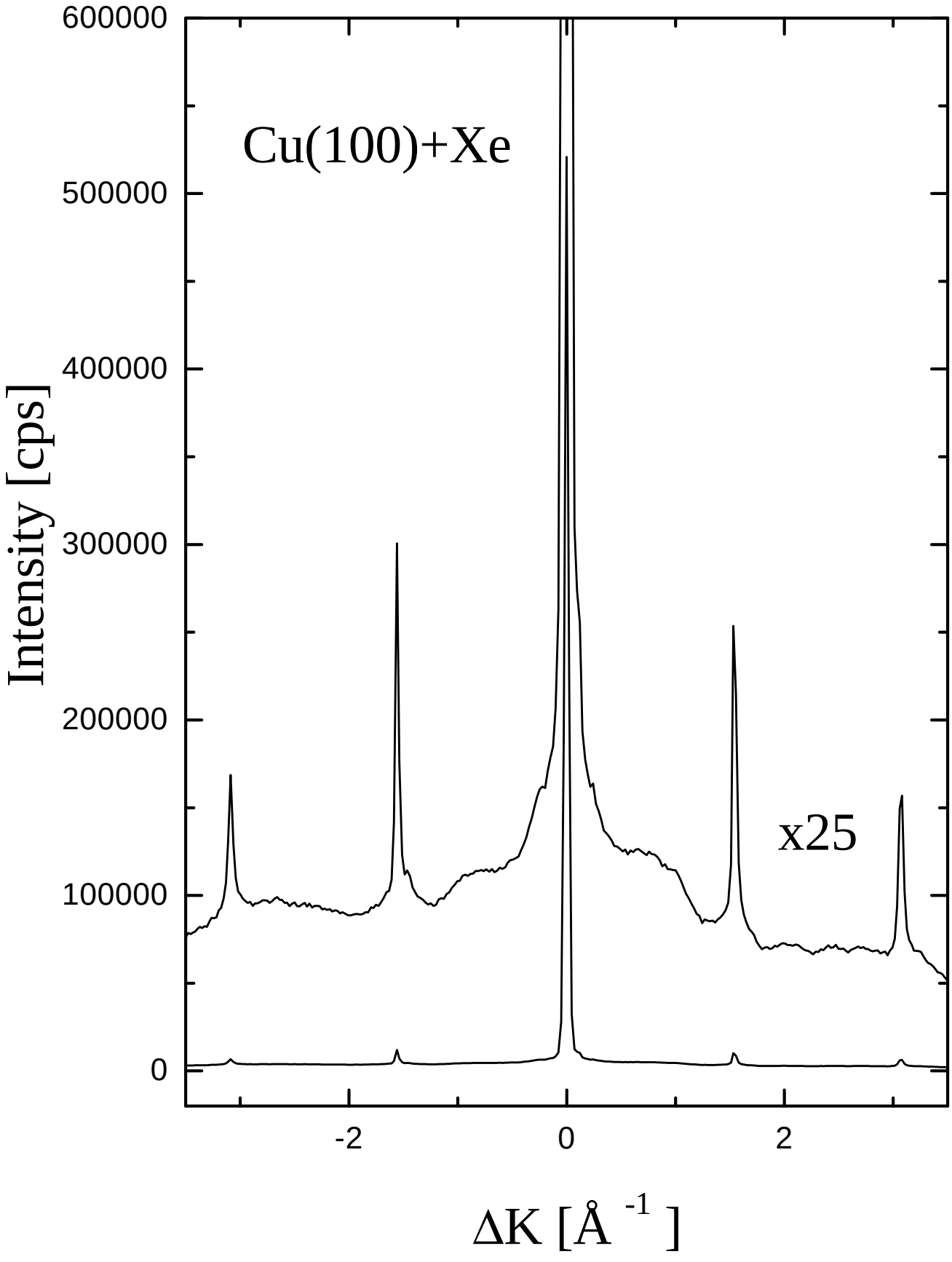
Cu(100)+Xe
x25
Intensity [cps]
600000
500000
400000
300000
200000
100000
0
-2
0
2
ΔK [Å -1]

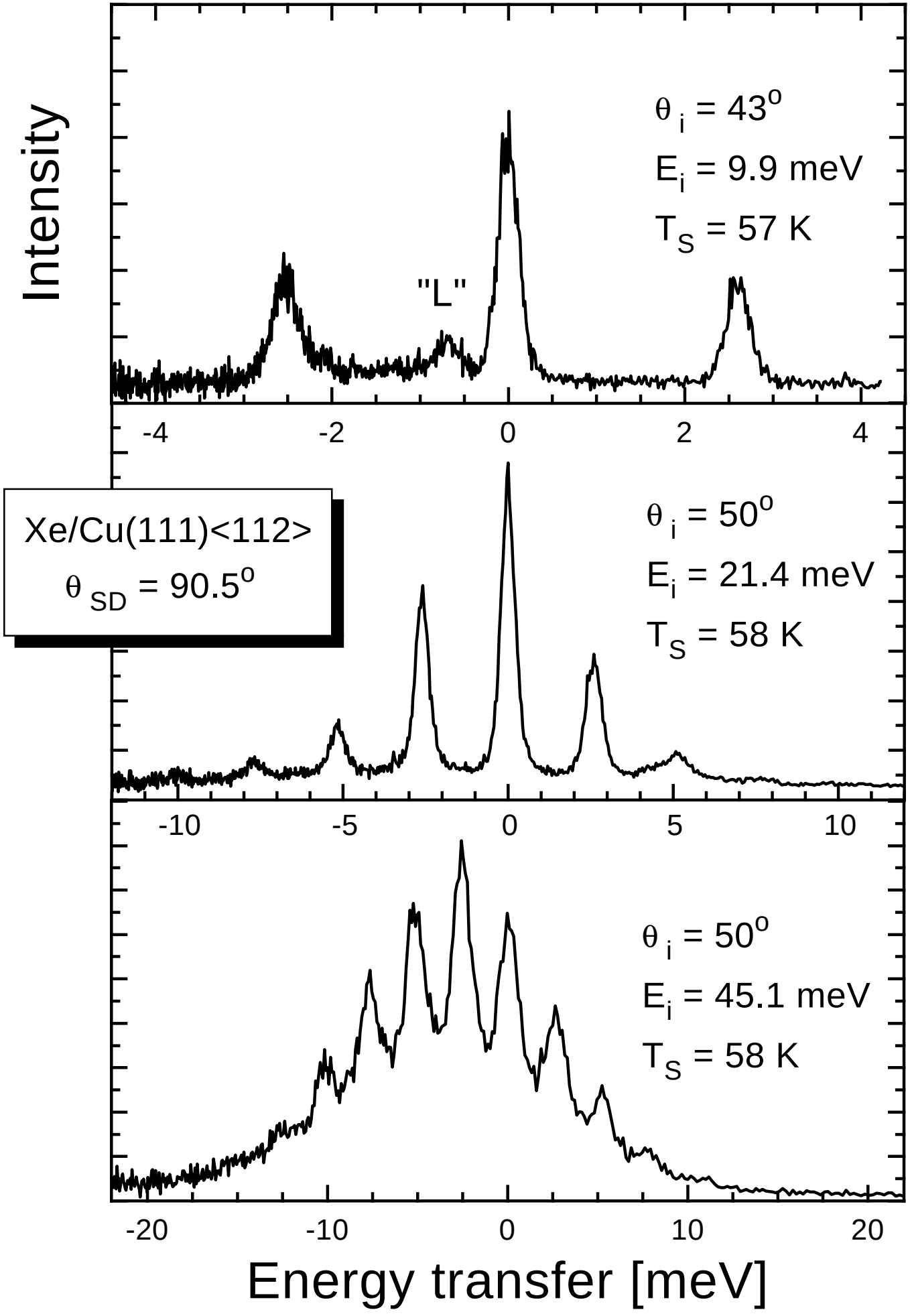
Intensity
θ i = 43o
Ei = 9.9 meV
TS = 57 K
"L"
-4
-2
0
2
4
Xe/Cu(111)<112>
θ SD = 90.5o
θ i = 50o
Ei = 21.4 meV
TS = 58 K
-10
-5
0
5
10
θ i = 50o
Ei = 45.1 meV
TS = 58 K
-20
-10
0
10
20
Energy transfer [meV]

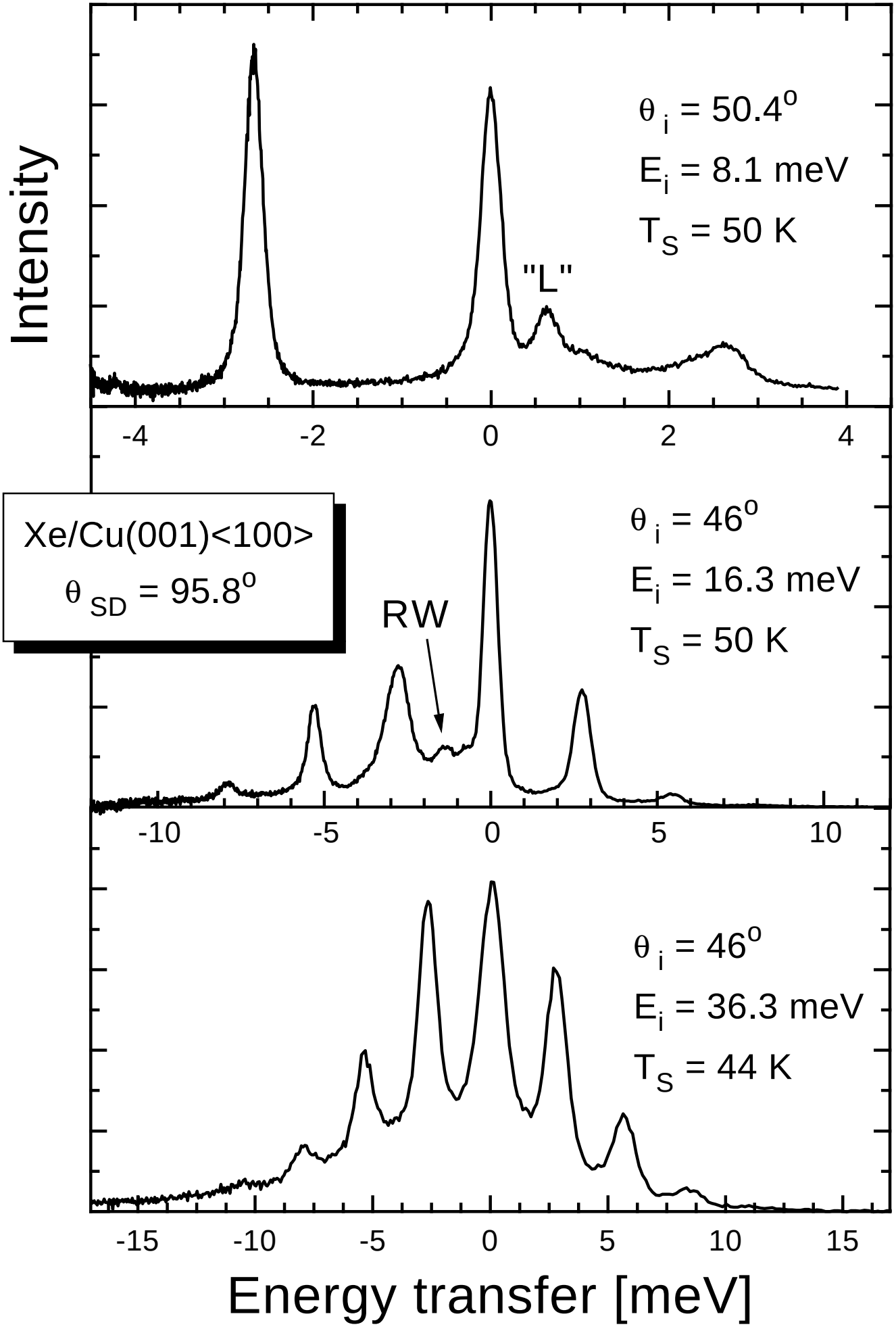
Intensity
θ i = 50.4o
Ei = 8.1 meV
TS = 50 K
"L"
-4
-2
0
2
4
Xe/Cu(001)<100>
θ SD = 95.8o
θ i = 46o
Ei = 16.3 meV
TS = 50 K
RW
-10
-5
0
5
10
θ i = 46o
Ei = 36.3 meV
TS = 44 K
-15
-10
-5
0
5
10
15
Energy transfer [meV]

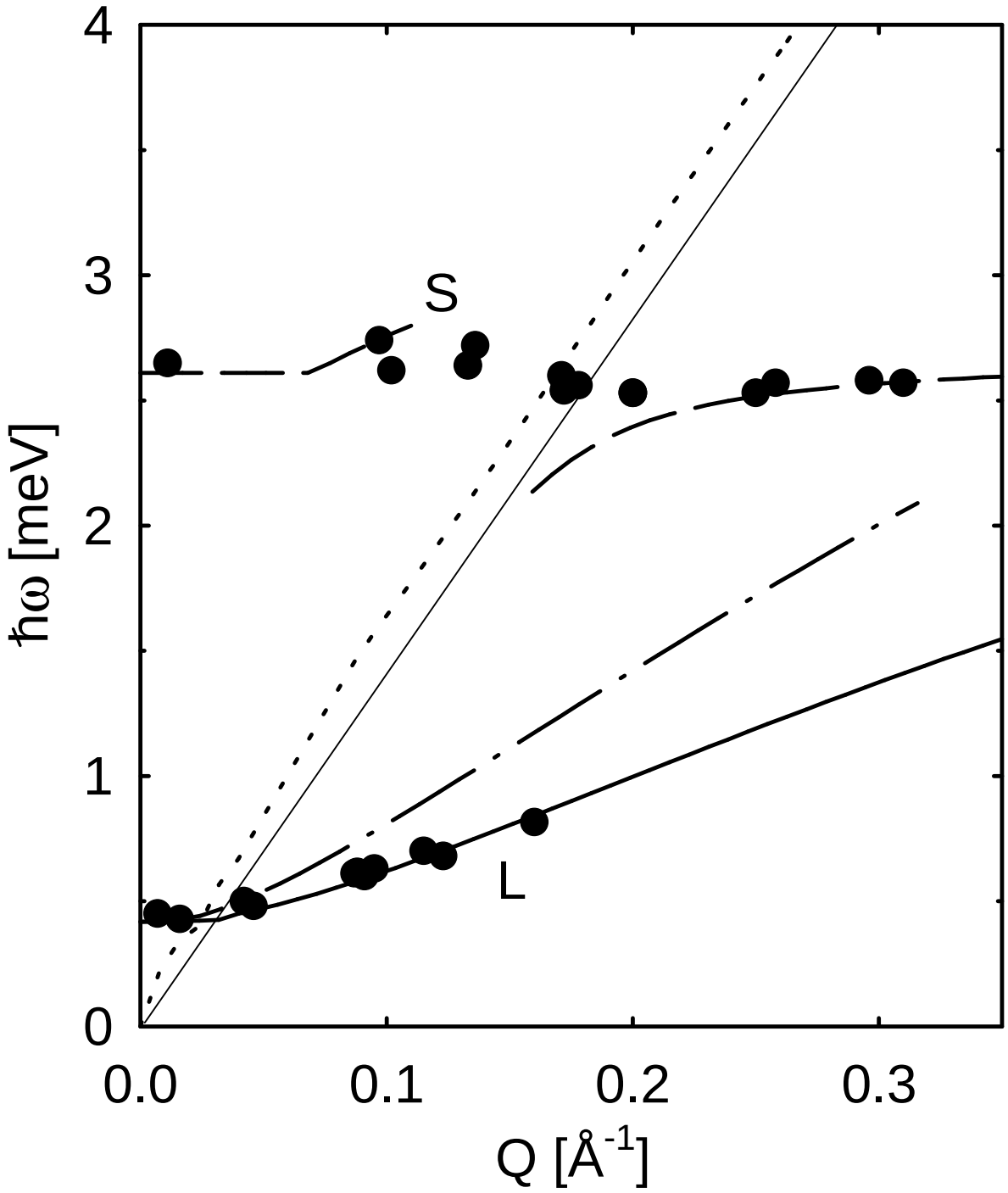
4
3
2
1
0
0.0
0.1
0.2
0.3
ħω [meV]
Q [Å^{-1}]
S
L

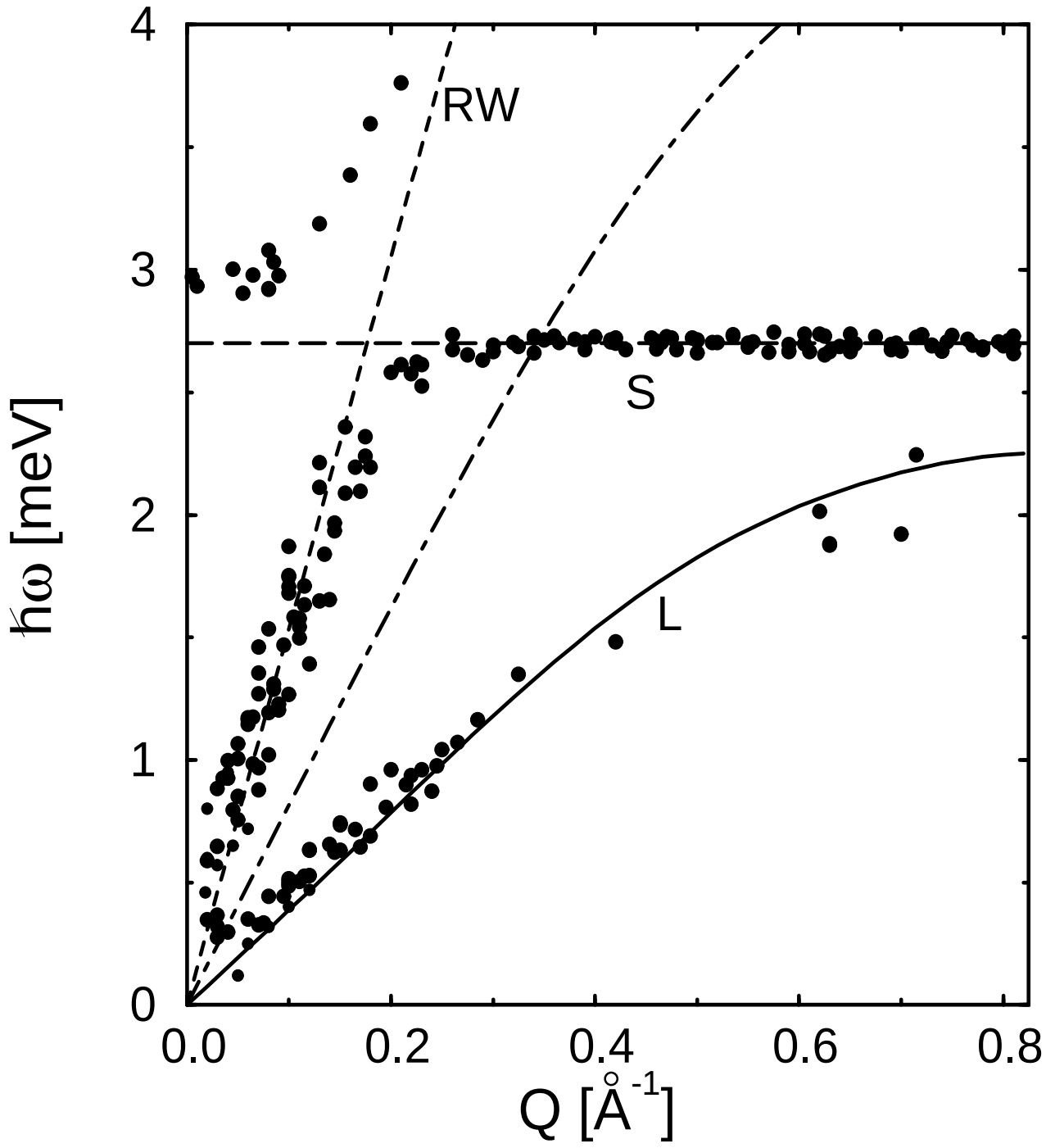
4
3
2
1
0
RW
S
L
ħω [meV]
0.0
0.2
0.4
0.6
0.8
Q [Å^{-1}]

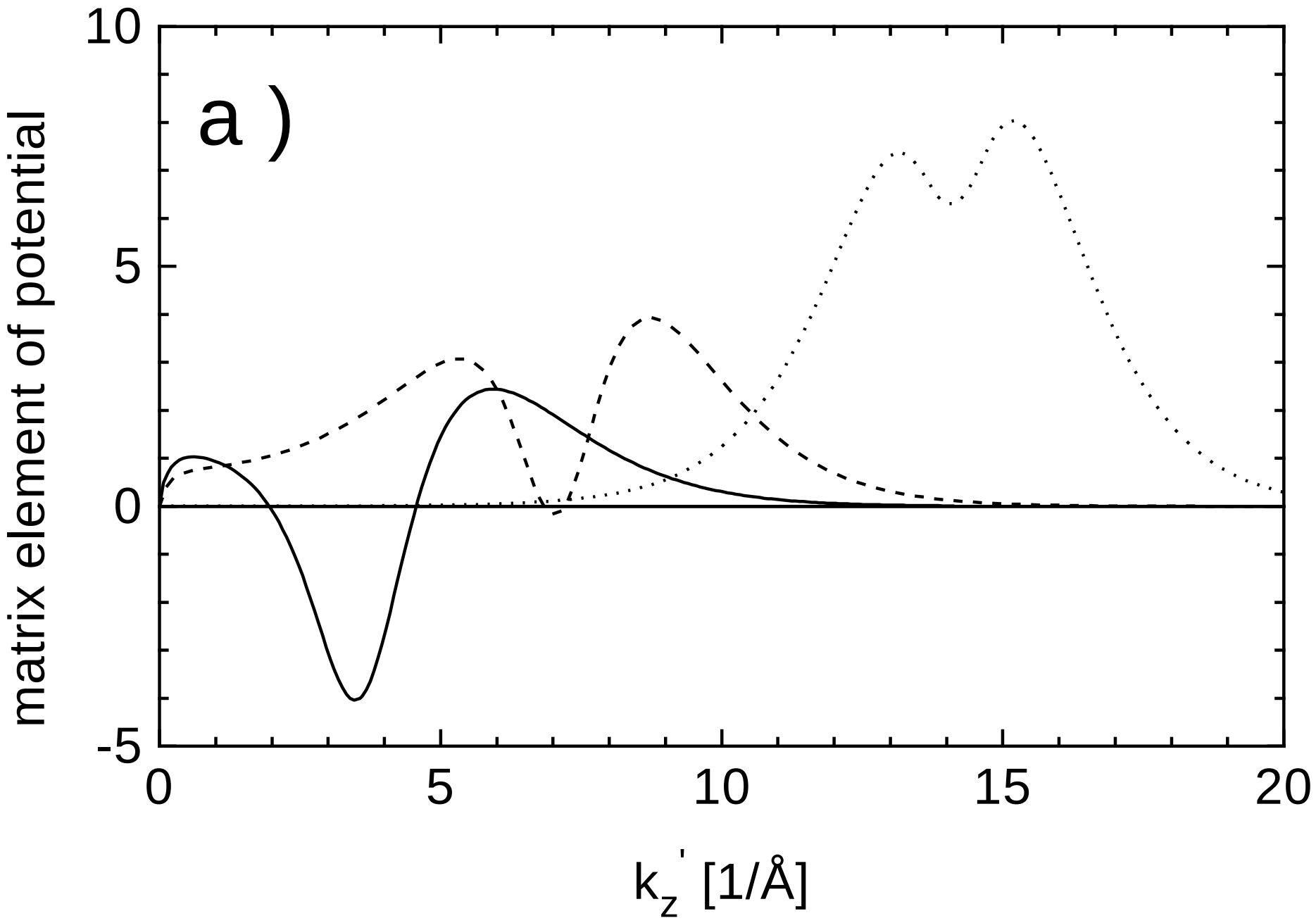
a)
matrix element of potential
10
5
0
-5
0
5
10
15
20
k_z' [1/Å]

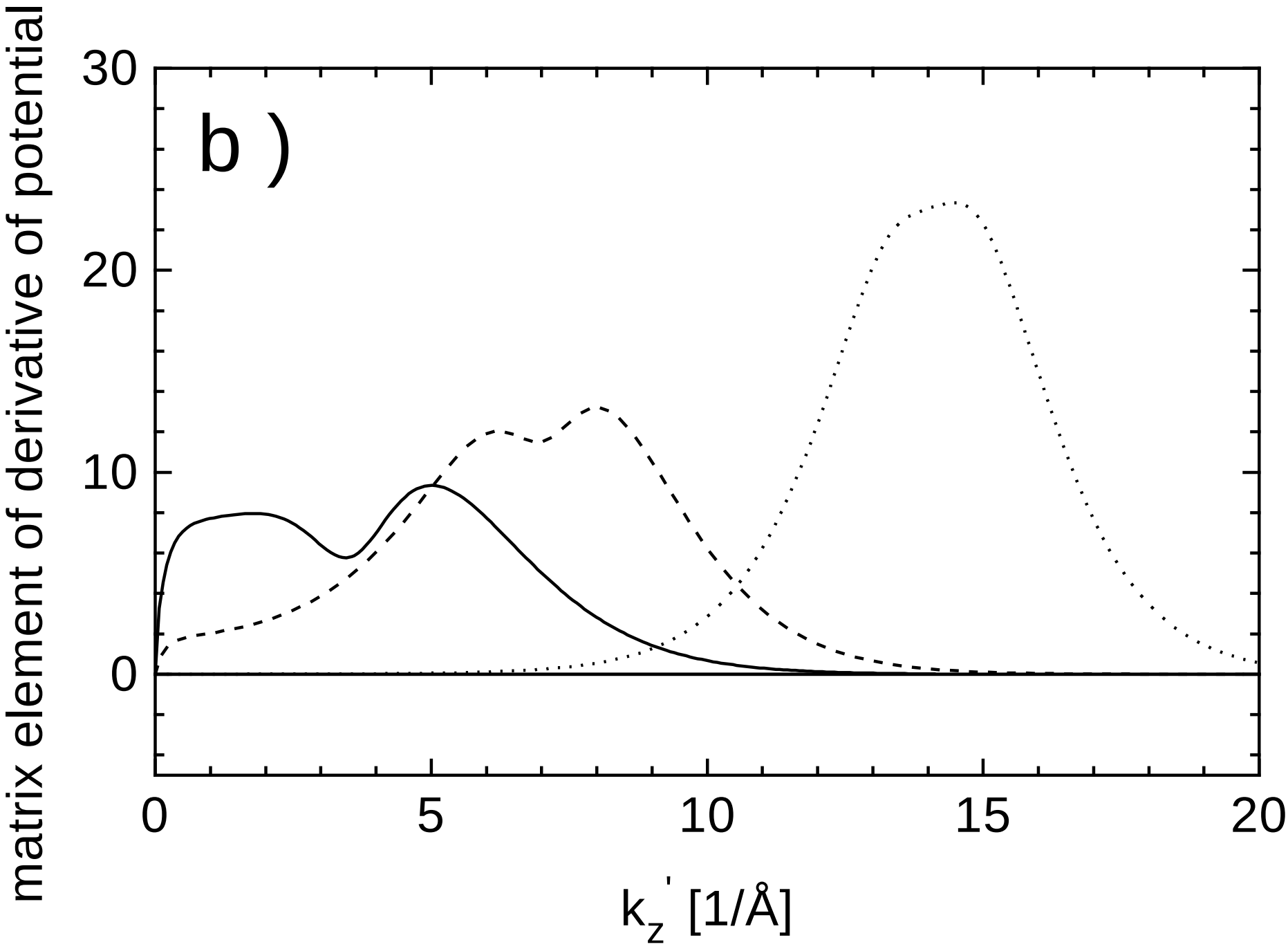
b)
matrix element of derivative of potential
30
20
10
0
0
5
10
15
20
k_z' [1/Å]

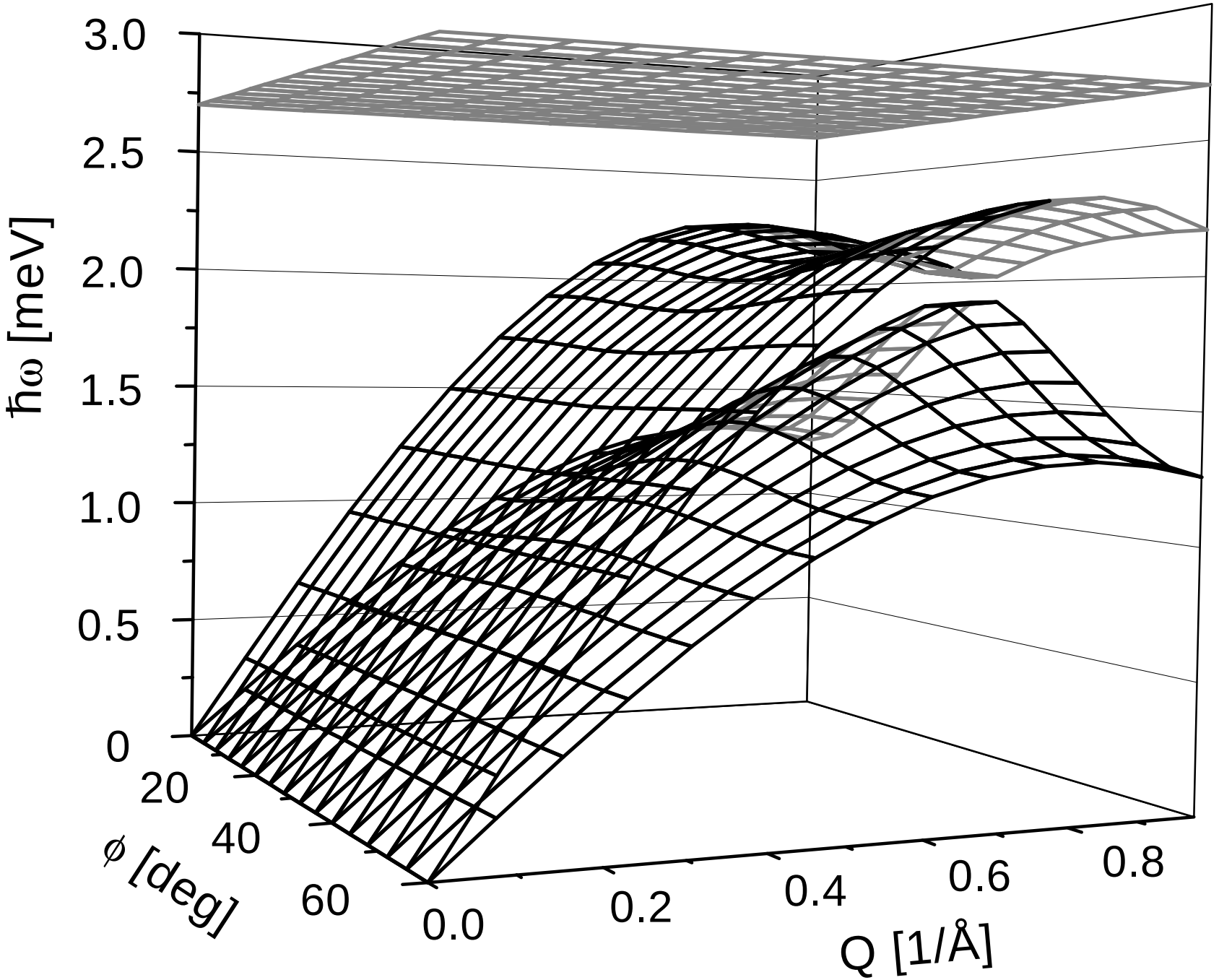
3.0
2.5
2.0
1.5
1.0
0.5
0
ħω [meV]
20
40
60
ϕ [deg]
0.0
0.2
0.4
0.6
0.8
Q [1/Å]

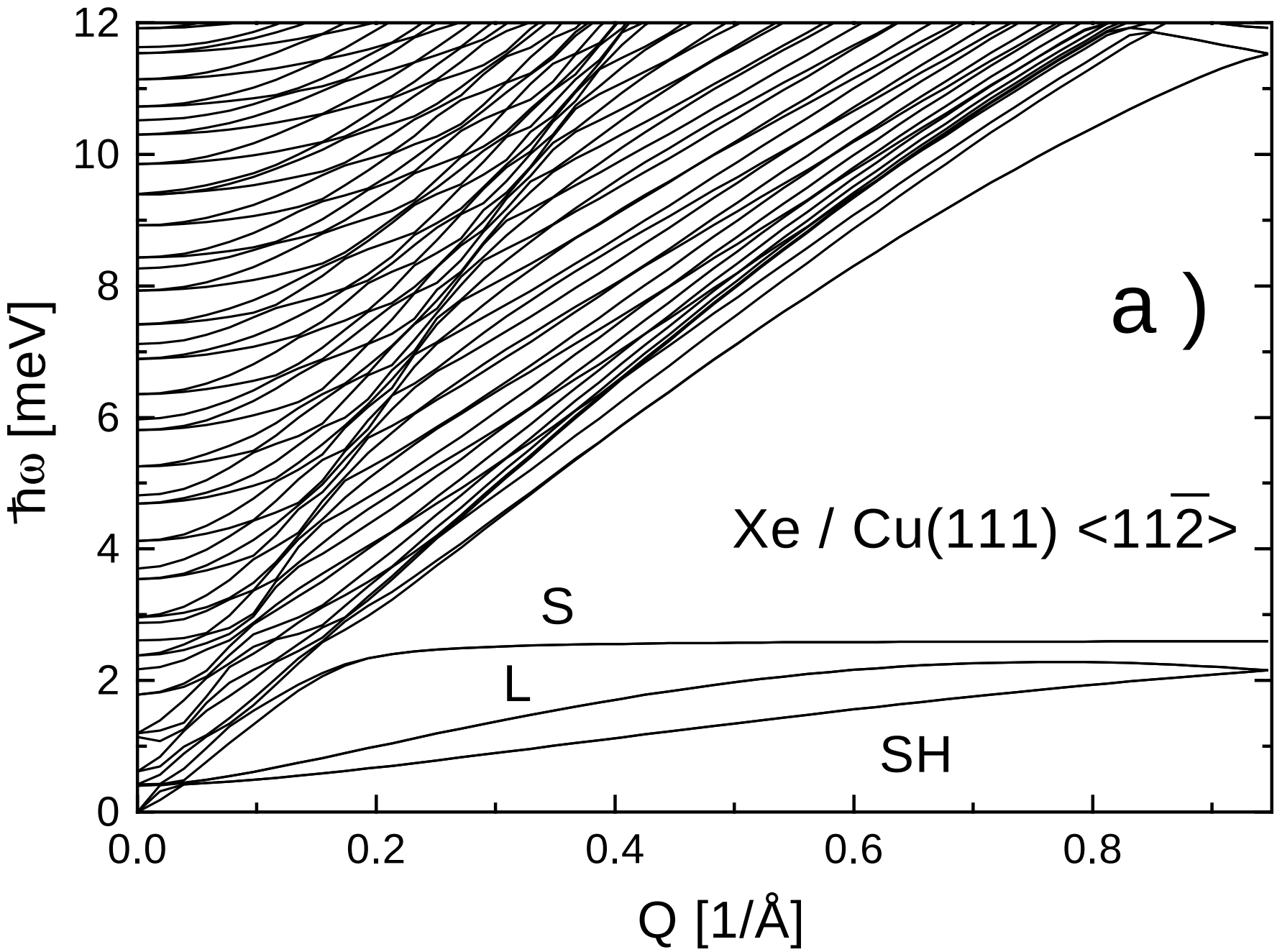
12
10
8
6
4
2
0
ħω [meV]
0.0
0.2
0.4
0.6
0.8
Q [1/Å]
a)
Xe / Cu(111) <11$\bar{2}$>
S
L
SH

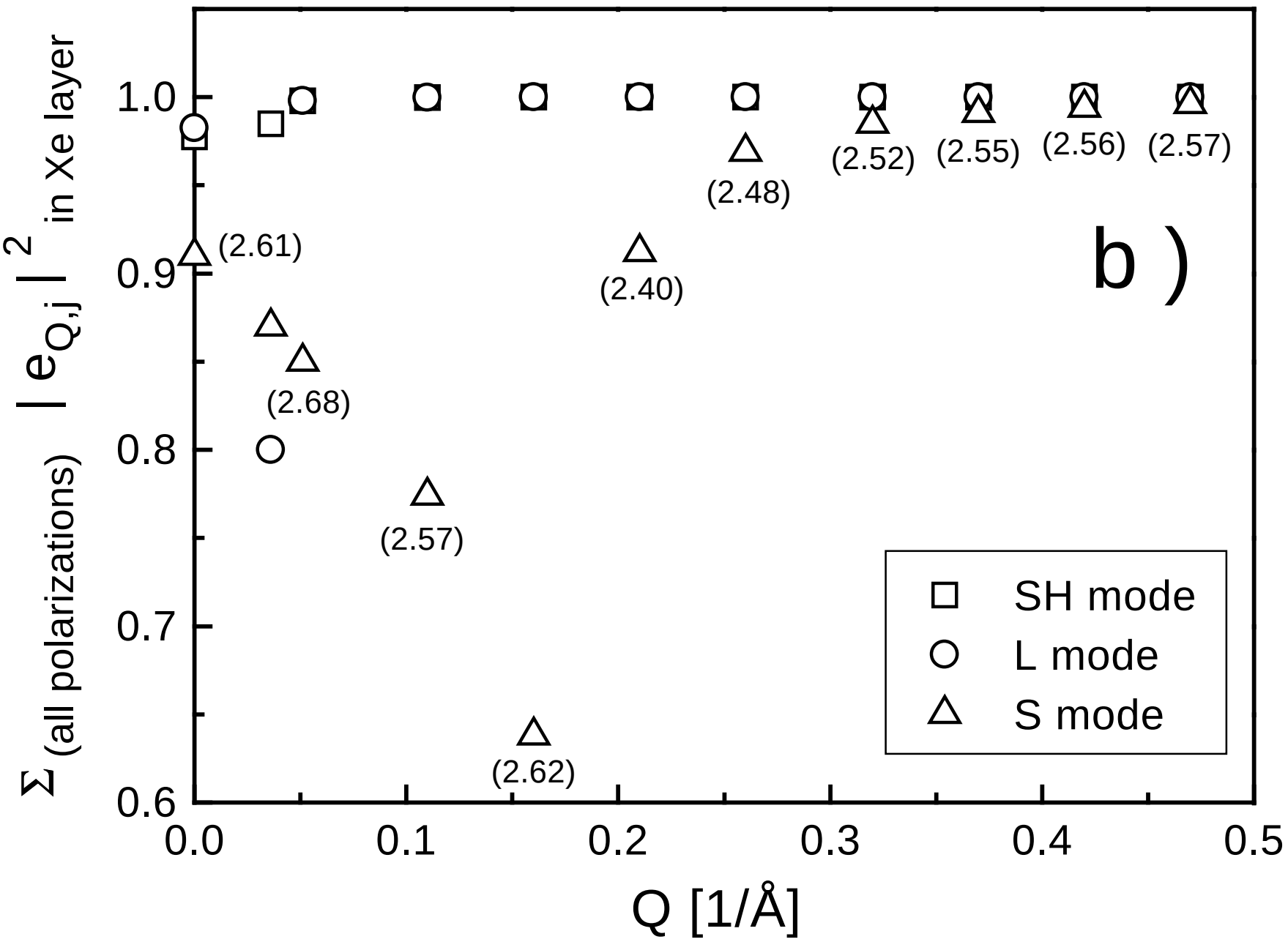
b)
(2.61)
(2.68)
(2.57)
(2.62)
(2.40)
(2.48)
(2.52)
(2.55)
(2.56)
(2.57)
SH mode
L mode
S mode
Σ (all polarizations) | e Q,j | 2 in Xe layer
Q [1/Å]
1.0
0.9
0.8
0.7
0.6
0.0
0.1
0.2
0.3
0.4
0.5

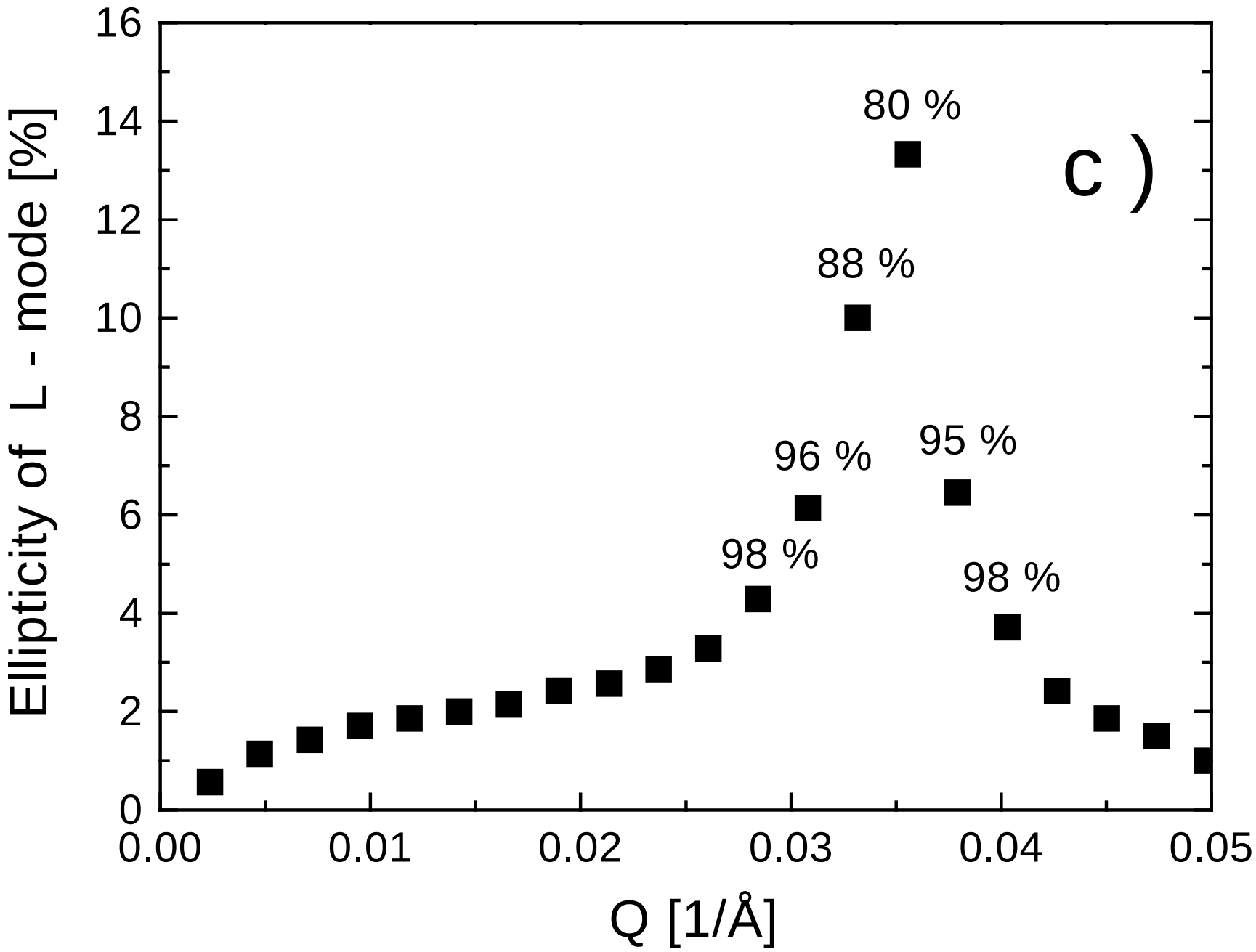
Ellipticity of L - mode [%]
Q [1/Å]
0
2
4
6
8
10
12
14
16
0.00
0.01
0.02
0.03
0.04
0.05
80 %
88 %
96 %
95 %
98 %
98 %
c)

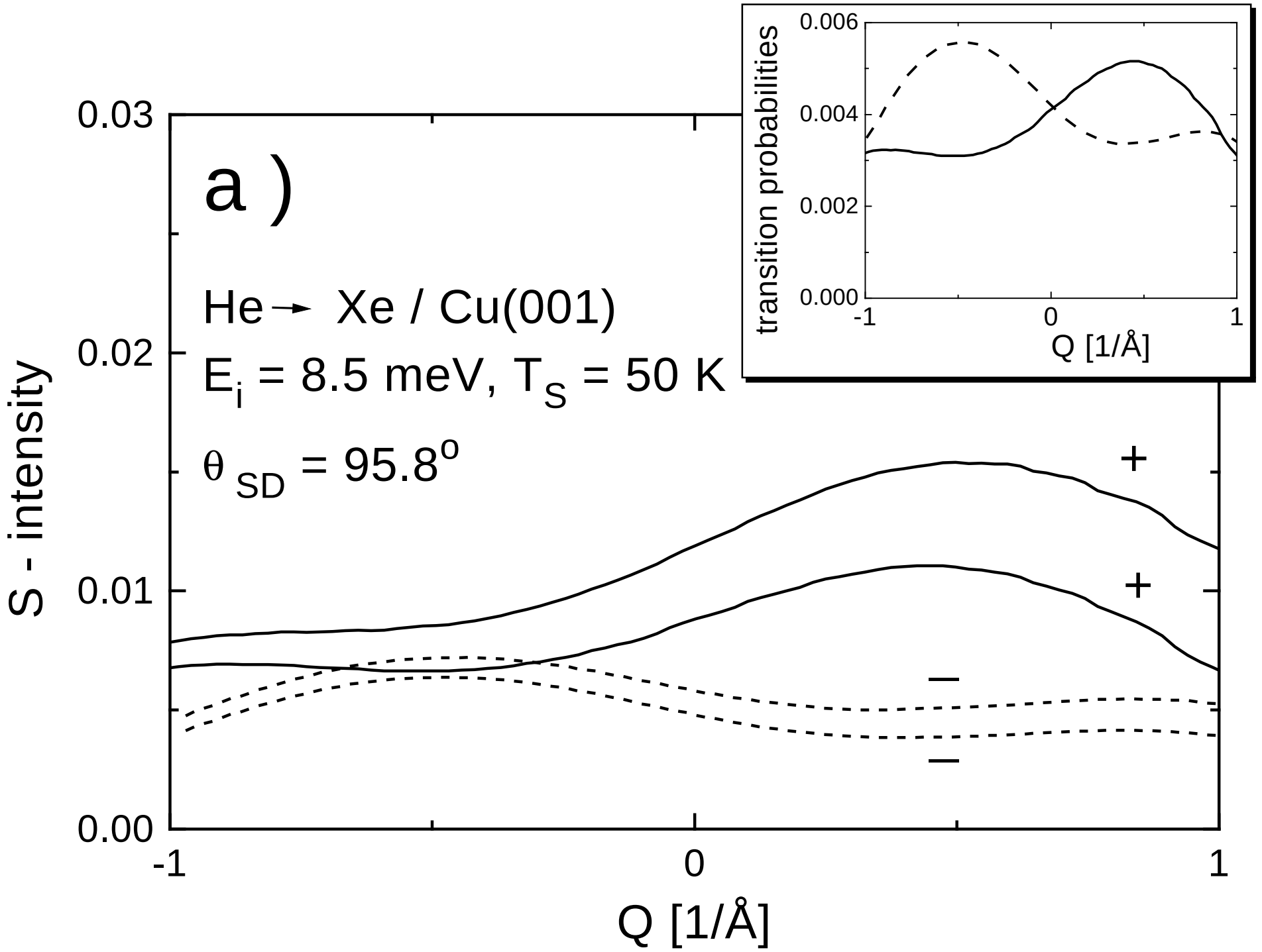
a)
He → Xe / Cu(001)
E_i = 8.5 meV, T_S = 50 K
θ_SD = 95.8°
S - intensity
Q [1/Å]
0.03
0.02
0.01
0.00
-1
0
1
+
+
−
−
transition probabilities
0.006
0.004
0.002
0.000
-1
0
1
Q [1/Å]

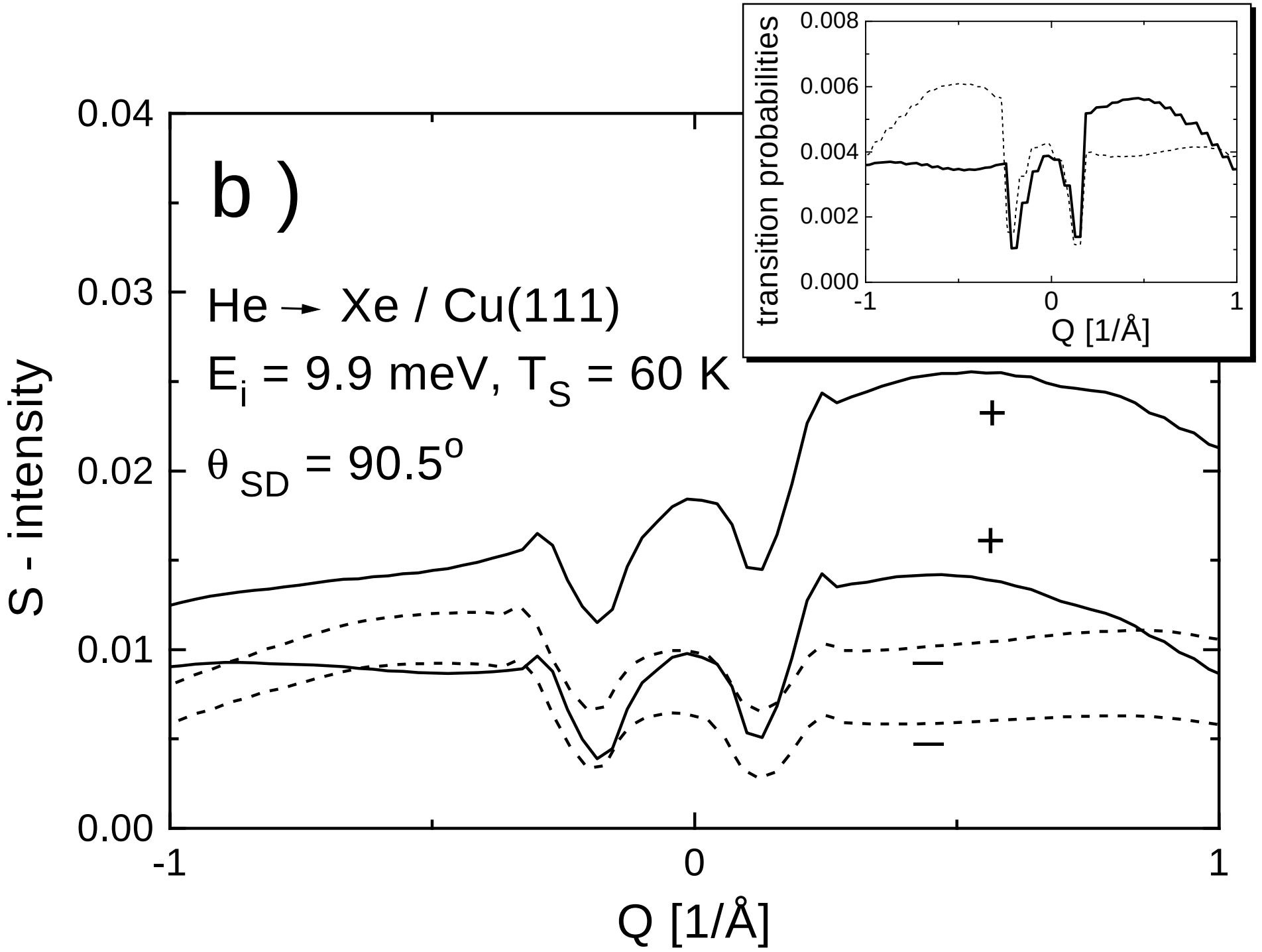
b)
He → Xe / Cu(111)
E_i = 9.9 meV, T_S = 60 K
θ_SD = 90.5°
S - intensity
Q [1/Å]
0.00
0.01
0.02
0.03
0.04
-1
0
1
+
+
−
−
transition probabilities
0.000
0.002
0.004
0.006
0.008
Q [1/Å]

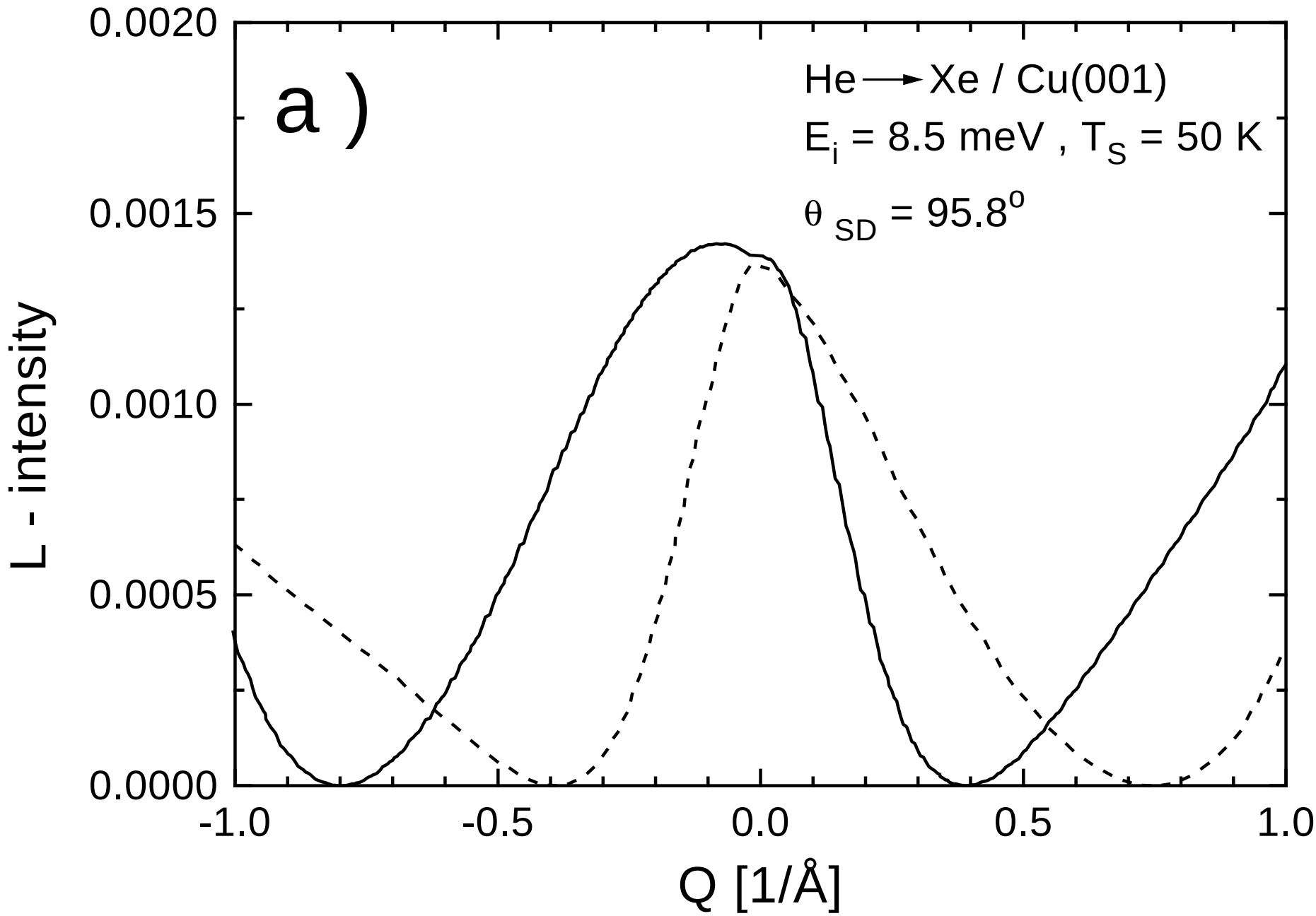
a)
He ⟶ Xe / Cu(001)
E_i = 8.5 meV , T_S = 50 K
θ_SD = 95.8°
L - intensity
Q [1/Å]
0.0020
0.0015
0.0010
0.0005
0.0000
-1.0
-0.5
0.0
0.5
1.0

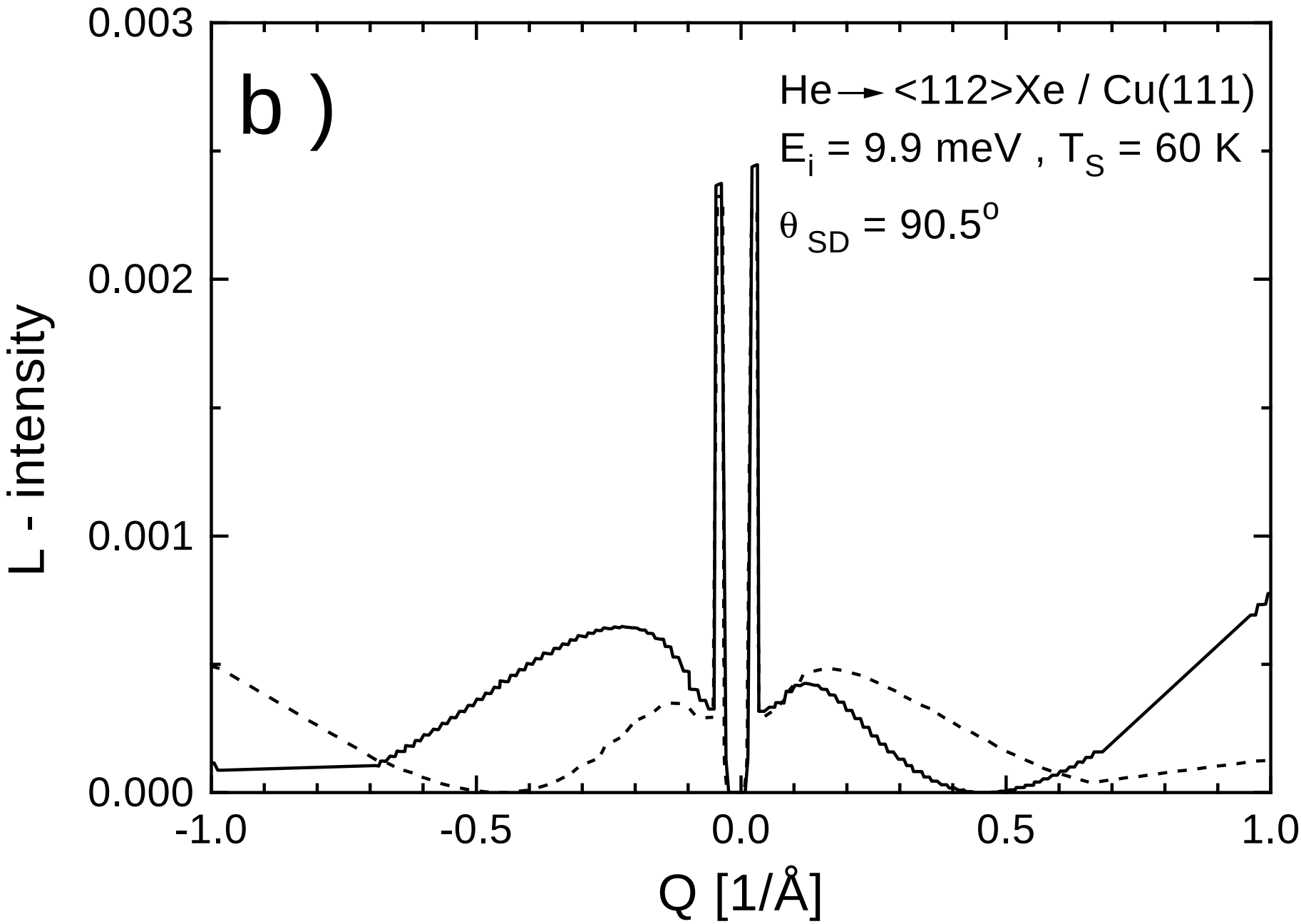
b)
He → <112>Xe / Cu(111)
E_i = 9.9 meV , T_S = 60 K
θ_SD = 90.5°
L - intensity
Q [1/Å]
0.003
0.002
0.001
0.000
-1.0
-0.5
0.0
0.5
1.0

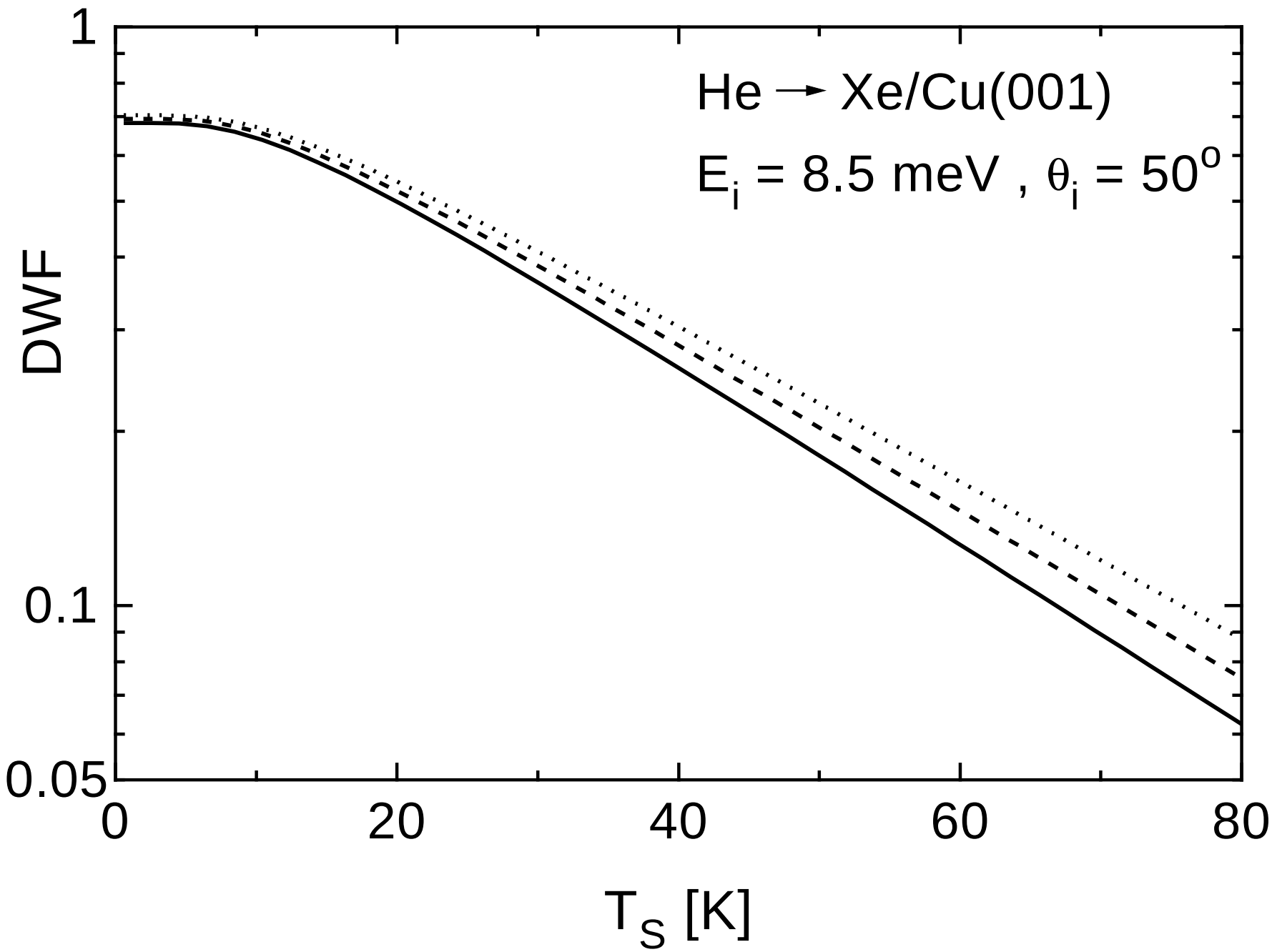
1
0.1
0.05
DWF
0
20
40
60
80
T_S [K]
He → Xe/Cu(001)
E_i = 8.5 meV , θ_i = 50^o

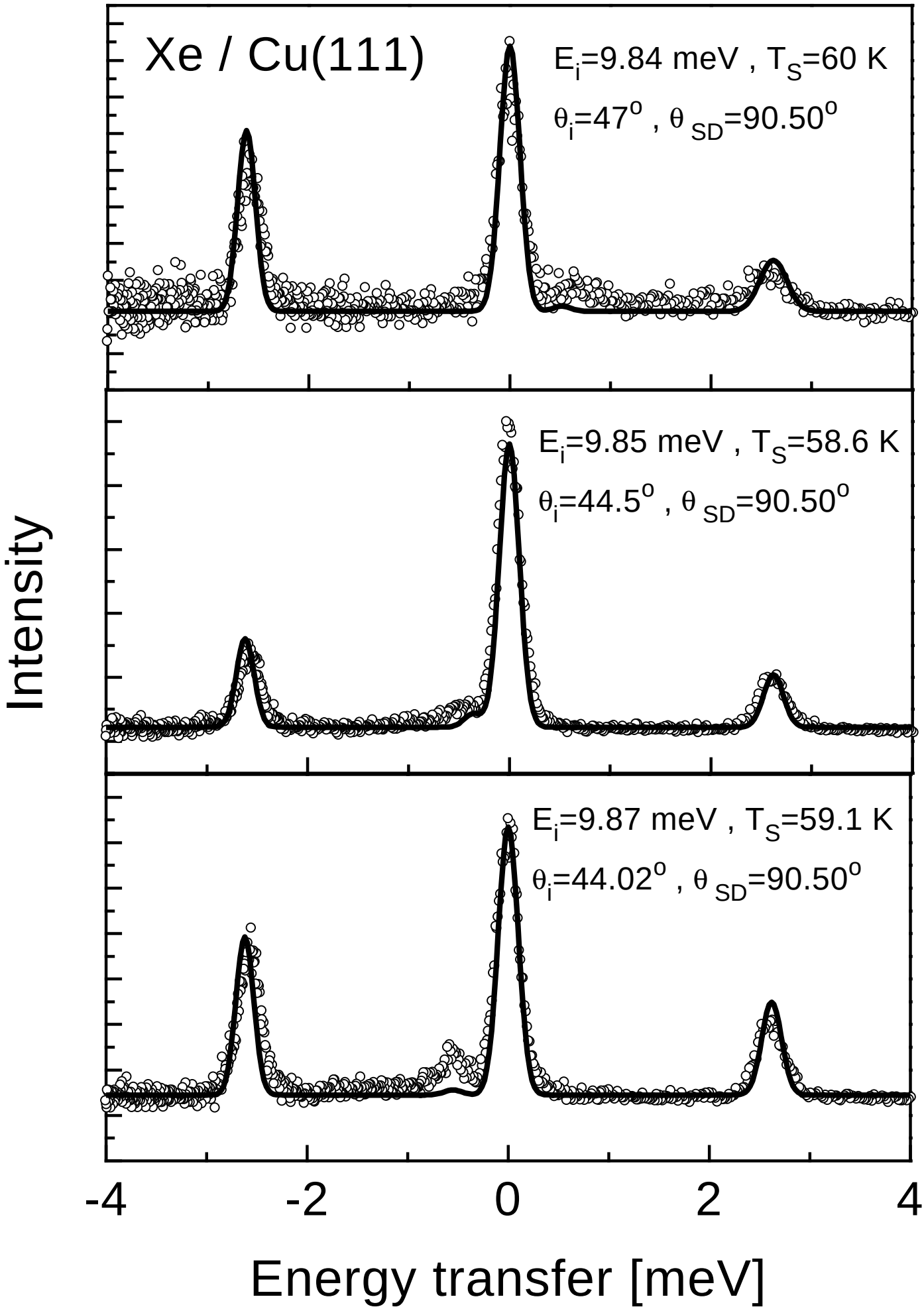
Xe / Cu(111)
E_i=9.84 meV , T_S=60 K
θ_i=47° , θ_SD=90.50°
E_i=9.85 meV , T_S=58.6 K
θ_i=44.5° , θ_SD=90.50°
E_i=9.87 meV , T_S=59.1 K
θ_i=44.02° , θ_SD=90.50°
Intensity
-4
-2
0
2
4
Energy transfer [meV]

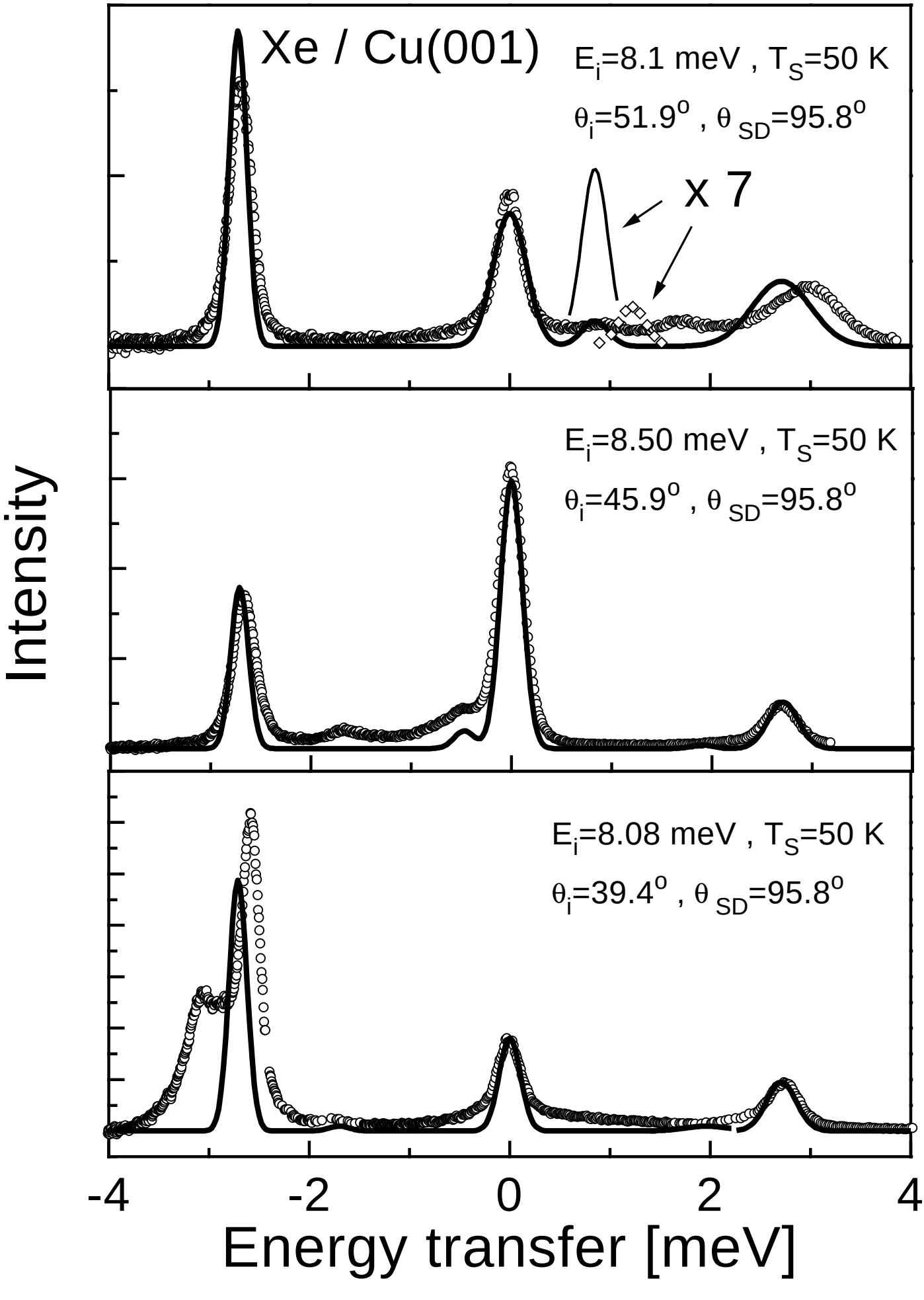
Xe / Cu(001)
E_i=8.1 meV , T_S=50 K
θ_i=51.9° , θ_SD=95.8°
x 7
E_i=8.50 meV , T_S=50 K
θ_i=45.9° , θ_SD=95.8°
E_i=8.08 meV , T_S=50 K
θ_i=39.4° , θ_SD=95.8°
Intensity
-4
-2
0
2
4
Energy transfer [meV]

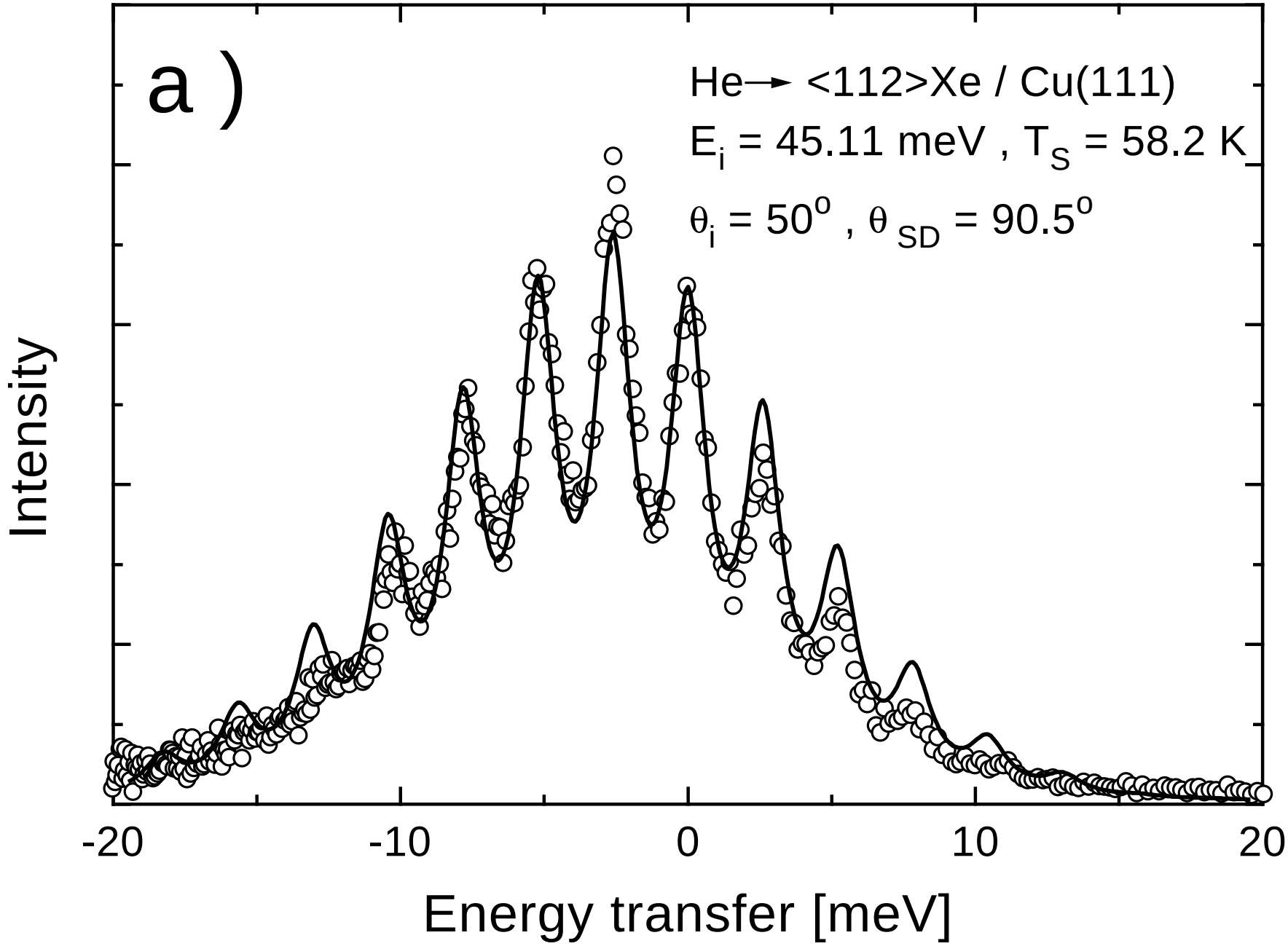
a)
He→ <112>Xe / Cu(111)
E_i = 45.11 meV , T_S = 58.2 K
θ_i = 50° , θ_SD = 90.5°
Intensity
-20
-10
0
10
20
Energy transfer [meV]

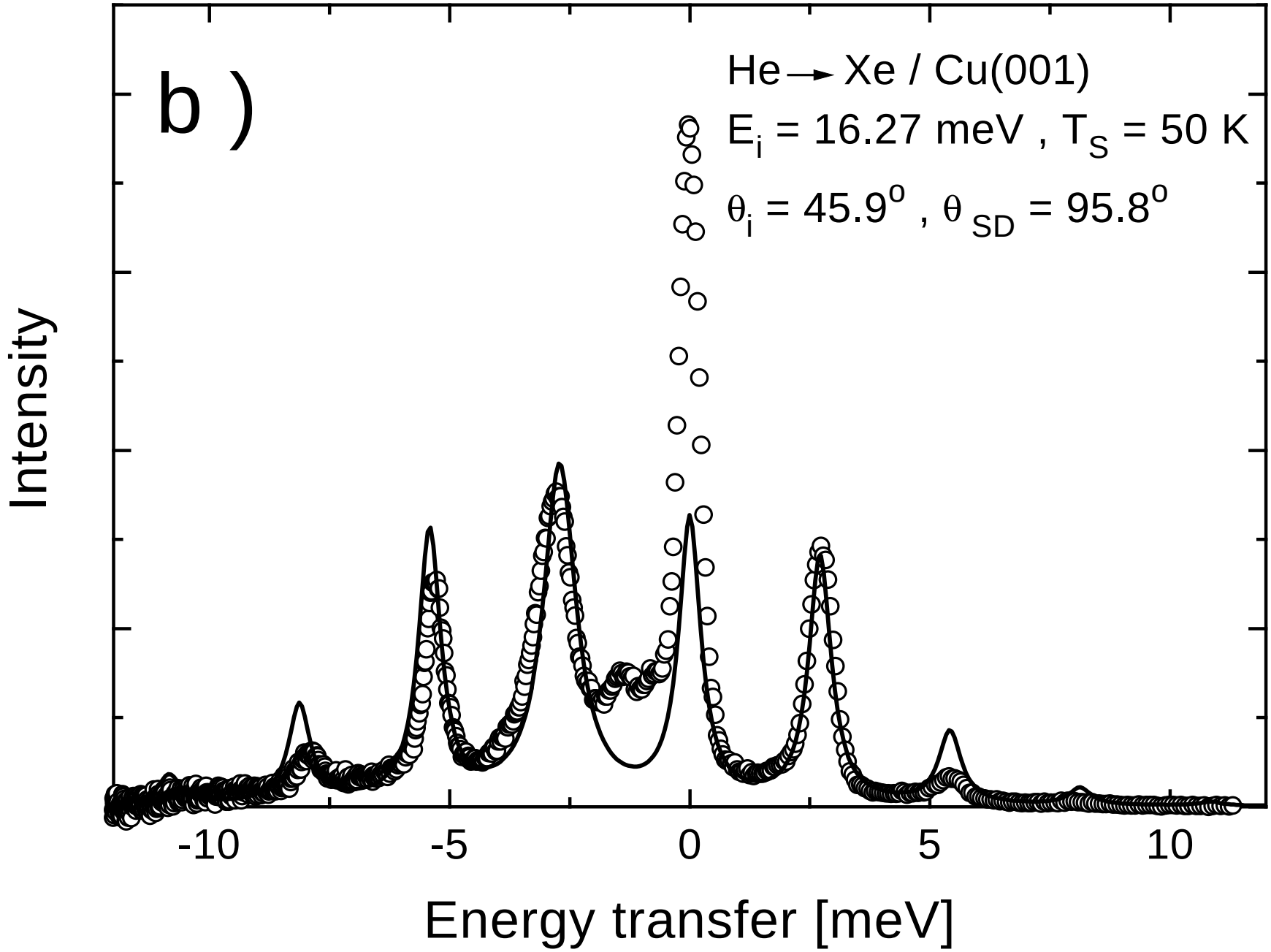
b)
He → Xe / Cu(001)
E_i = 16.27 meV , T_S = 50 K
θ_i = 45.9° , θ_SD = 95.8°
Intensity
-10
-5
0
5
10
Energy transfer [meV]